frontiers in Earth Science

ORIGINAL RESEARCH
published: 24 January 2019
doi: 10.3389/feart.2018.00238

Isotopic and Petrologic Investigation, and a Thermomechanical Model of Genesis of Large-Volume Rhyolites in Arc Environments: Karymshina Volcanic Complex, Kamchatka, Russia

Ilya N. Bindeman[1], Vladimir L. Leonov[2], Dylan P. Colón[1], Aleksey N. Rogozin[2], Niccole Shipley[1], Brian Jicha[3], Matthew W. Loewen[1,4] and Taras V. Gerya[5]*

[1] Department of Earth Sciences, University of Oregon, Eugene, OR, United States, [2] Institute of Volcanology and Seismology, Petropavlovsk-Kamchatsky, Russia, [3] Department of Geoscience, University of Wisconsin, Madison, WI, United States, [4] U.S. Geological Survey, Alaska Volcano Observatory, Anchorage, AK, United States, [5] Department of Earth Sciences, ETH Zurich, Zurich, Switzerland

OPEN ACCESS

Edited by:
Katherine Dobson, Durham University, United Kingdom

Reviewed by:
Marlina A. Elburg, University of Johannesburg, South Africa
Michel Grégoire, Center for the National Scientific Research (CNRS), France

***Correspondence:**
Ilya N. Bindeman
bindeman@uoregon.edu

Specialty section:
This article was submitted to Petrology, a section of the journal Frontiers in Earth Science

Received: *08 October 2018*
Accepted: *10 December 2018*
Published: *24 January 2019*

Citation:
Bindeman IN, Leonov VL, Colón DP, Rogozin AN, Shipley N, Jicha B, Loewen MW and Gerya TV (2019) Isotopic and Petrologic Investigation, and a Thermomechanical Model of Genesis of Large-Volume Rhyolites in Arc Environments: Karymshina Volcanic Complex, Kamchatka, Russia. Front. Earth Sci. 6:238. doi: 10.3389/feart.2018.00238

The Kamchatka Peninsula of eastern Russia is currently one of the most volcanically active areas on Earth where a combination of >8 cm/yr subduction convergence rate and thick continental crust generates large silicic magma chambers, reflected by abundant large calderas and caldera complexes. This study examines the largest center of silicic 4-0.5 Ma Karymshina Volcanic Complex, which includes the 25 × 15 km Karymshina caldera, the largest in Kamchatka. A series of rhyolitic tuff eruptions at 4 Ma were followed by the main eruption at 1.78 Ma and produced an estimated 800 km^3 of rhyolitic ignimbrites followed by high-silica rhyolitic post-caldera extrusions. The postcaldera domes trace the 1.78 Ma right fracture and form a continuous compositional series with ignimbrites. We here present results of a geologic, petrologic, and isotopic study of the Karymshina eruptive complex, and present new Ar-Ar ages, and isotopic values of rocks for the oldest pre- 1.78 Ma caldera ignimbrites and intrusions, which include a diversity of compositions from basalts to rhyolites. Temporal trends in $\delta^{18}O$, $^{87}Sr/^{86}Sr$, and $^{144}Nd/^{143}Nd$ indicate values comparable to neighboring volcanoes, increase in homogeneity, and temporal increase in mantle-derived Sr and Nd with increasing differentiation over the last 4 million years. Data are consistent with a batholithic scale magma chamber formed by primarily fractional crystallization of mantle derived composition and assimilation of Cretaceous and younger crust, driven by basaltic volcanism and mantle delaminations. All rocks have 35–45% quartz, plagioclase, biotite, and amphibole phenocrysts. Rhyolite-MELTS crystallization models favor shallow (2 kbar) differentiation conditions and varying quantities of assimilated amphibolite partial melt and hydrothermally-altered silicic rock. Thermomechanical modeling with a typical 0.001 km^3/yr eruption rate of hydrous basalt into a 38 km Kamchatkan arc crust produces two magma bodies, one near the Moho and the other engulfing the entire section of upper crust. Rising basalts are trapped in the lower portion of an upper crustal magma body, which exists in a partially molten to solid state. Differentiation products of basalt periodically mix with the resident magma diluting its crustal isotopic signatures.

At the end of the magmatism crust is thickened by 8 km. Thermomechanical modeling show that the most likely way to generate large spikes of rhyolitic magmatism is through delamination of cumulates and mantle lithosphere after many millions of years of crustal thickening. The paper also presents a chemical dataset for Pacific ashes from ODDP 882 and 883 and compares them to Karymshina ignimbrites and two other Pleistocene calderas studied by us in earlier works.

Keywords: high-silica rhyolites, oxygen isotopes (18O), thermomechanical modeling, caldera, Ar-Ar dating, Sr isotopes, Nd isotopes, Kamchatka (Russia)

INTRODUCTION

Voluminous silicic volcanism in island arcs worldwide is a reflection of the production of silicic magmas by mafic magma differentiation and crustal anatexis, and of the crustal redistribution of silicic and mafic materials, which segregates the crust into deep mafic and shallow silicic compositional domains (Vogel et al., 2006; Vogt et al., 2012). Together with arc accretion to continental margins, these processes have contributed to the growth, segregation, and differentiation of continental crust throughout geologic history (Taylor and McLennan, 1995; Rudnick and Gao, 2003). There is always a chicken-and-egg question in continental arcs however, on whether silicic magmas arise via magmatic differentiation, especially in arcs with high convergence rates such as Kamchatka, the Andes, and Japan, or if silicic magmatism occurs because felsic rocks are initially present in preexisting continental crust (Tatsumi, 2005; Winter, 2010). Additionally, continental arcs with older crust are isotopically distinct and this isotopic torque permits the better recognition of the petrogenetic processes that may similarly operate in juvenile oceanic arcs (Hildreth and Moorbath, 1988). Anatexis and remelting of the preexisting silicic crust in continental arcs produce conditions where further segregation of silicic differentiates and partial melts leads to redistribution of silicic components to the upper crust in a positive feedback of crust-building (Bindeman and Simakin, 2014). Isotope geochemistry, petrology, and large-scale thermomechanical modeling serve as tools to address these questions (Tatsumi, 2005; Eichelberger et al., 2006; Winter, 2010; Vogt et al., 2012). Island arcs, and especially continental arcs, that are built on thick crust often display continuous silicic magmatism in one segment of the arc lasting many millions of years, which can be expressed on the surface by overlapping caldera collapses (de Silva and Gosnold, 2007). In other conditions, voluminous silicic magmas appear suddenly without prolonged preconditioning of the crust, and magmatism remains bimodal with basaltic and rhyolitic peaks (Kimura et al., 2015).

The Kamchatka Peninsula in northeast Russia represents the most volcanically active segment of the Pacific Ring of fire, due to in part to fast >8 cm/yr orthogonal subduction with a thick crust in the overriding plate (**Figure 1**, Ponomareva et al., 2007). The eastern margin is constructive with a series of arcs accreting to Kamchatka in the Cenozoic (Konstantinovskaia, 2001; Hourigan et al., 2009) and now forming the basement under the modern volcanic edifices. The last episode of arc-continent collision lasted from 7 to 12 Ma (Lander and Shapiro, 2007; Scholl, 2007). High magma accumulation rates coupled with rapid uplift due to compressional forearc forces leads to the exposure of various basement rocks within the modern arc, providing insights into the arc structure (**Figures 1**, **2**). These include Cretaceous-Eocene metamorphic rocks, 11 Ma granitic bodies exposed on the Pacific shore such as Akhomten Massif, and younger volcanic sequences (Seligman et al., 2014). More volcanic calderas occur in Kamchatka than any other arc worldwide (Bindeman et al., 2010), with examples of both systems with continuous compositional variation in erupted material, as well as of the bimodal end member. An example of the latter is the large Pauzhetka caldera in southernmost Kamchatka, where the crust is the thinnest and consists mostly of greywackes and basalts.

This study mostly focuses on a series of voluminous 4.11–0.50 Ma rhyolites and high-silica rhyolites (HSR) erupted as voluminous ignimbrites and lavas that we collectively refer to as the Karymshina Volcanic Complex (KVC) (**Figures 1**, **2**). The KVC is likely the largest center of silicic volcanism in Kamchatka as is established here. Abundant silicic rocks were first discovered in the area in the course of geologic mapping in the 1960s—1980s and were initially considered to represent several eruptive silicic vents collectively forming a volcano-tectonic depression (Sheimovich and Patoka, 1989; Sheimovich and Khatskin, 1996; Geological Map of the Russian Federation, 2000; Sheimovich and Golovin, 2003). A part of this complex around Tolsty Mys Mountain (1343 m), the highest topographic point in the area (**Figure 2**), was reinterpreted by Leonov and Rogozin (2007) as a resurgent dome inside an uplifted and dissected, hundreds of meters-thick intracaldera tuff, within the large 25 × 15 km Karymshina Caldera. Bindeman et al. (2010) performed Ar-Ar and U-Pb zircon dating and demonstrated that the top and the bottom of the 1,000 m ignimbrite sheet (their **Figure 4**), have identical ages of 1.78 ± 0.02 Ma. Due to the great thickness and lateral extent of this deposit (**Figure 2**), these authors agreed with interpretation of Leonov and Rogozin (2007) that it represents a remnant of densely welded and relatively compositionally unzoned 1.78 Ma intracaldera ignimbrite, brought up by post 1.78 Ma uplift and erosion. The situation is analogous to the 2.8 Ma, two-km thick uplifted and dissected, intracaldera Chegem ignimbrite in the Caucasus and we take instruction from the study of that center by Lipman et al. (1993) in describing and discerning field relations for Karymshina ignimbrite. The search for an identical in age 1.78 Ma extracaldera ignimbrite in past 10 years is still ongoing; this is partly explained by

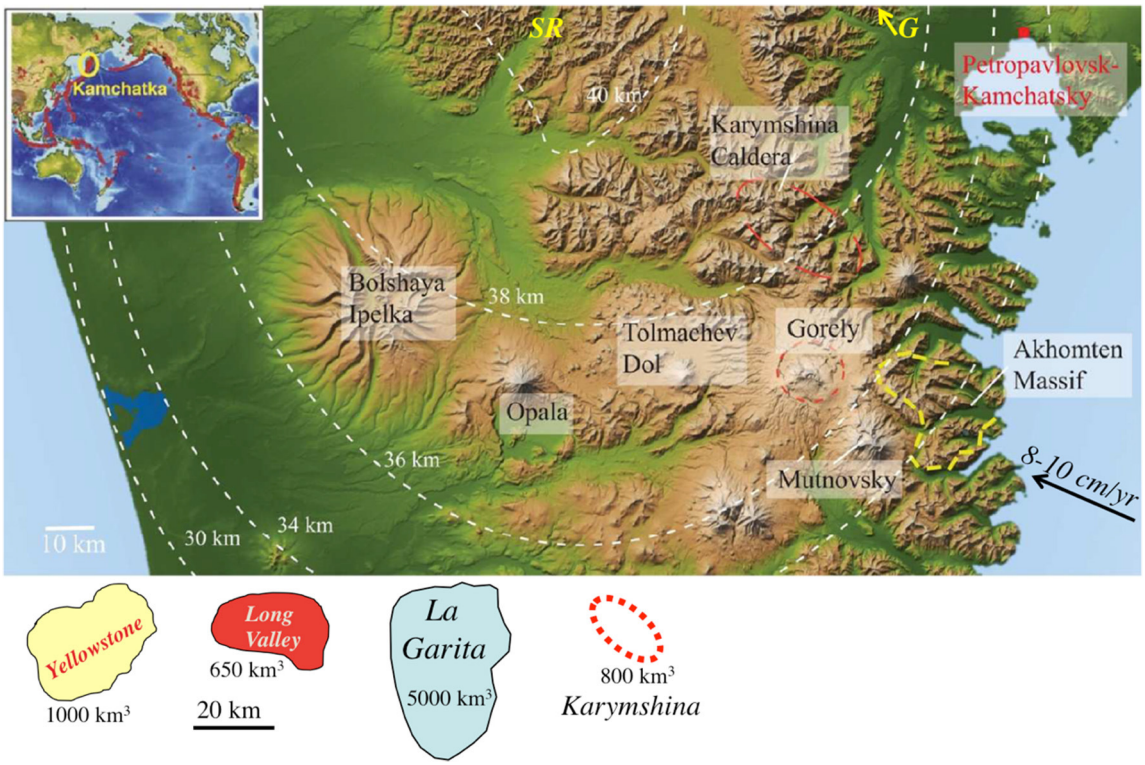

FIGURE 1 | Karymshina Volcanic Complex in Kamchatka. Inset: plate tectonic configuration, and presently active volcanoes of the Eastern Volcanic Front, and extinct volcanic arc in the Sredinny Range. A cross section through south-central Kamchatka shows Karymshina Volcanic Complex and other neighboring volcanoes mentioned in text. Notice uplift and topographic manifestation of Late Pleistocene calderas (e.g., Gorely), ignimbrite sheets around it and glacial coastal fjords and erosional features. Crustal thickness is shown my dashed line from Baboshina et al. (2000). Ganal metamorphic basement (G) with mafic amphibolites of Cretaceous age is to the NW of the letter G, while Sredinny Range with siliceous gneisses extends north of the letter SR. Lower panel shows comparison of caldera outlines mentioned in text and their eruptive volumes.

uplift and erosion, dense vegetation in Kamchatka and difficult logistics. The similarly uplifted and eroded Chegem tuff still preserves scattered outcrops of ~50 m thick extracaldera Chegem ignimbrite only in the immediate vicinity of caldera (Lipman et al., 1993). Search for an extracaldera 1.78 Ma Karymshina tuff and dating efforts resulted in the discovery of both older and younger, dacitic and rhyolitic tuffs and new extrusions ranging in age from 4.11 to 1.39 Ma (Bindeman et al., 2010, and this study, **Figure 2** and **Table 2**).

Geophysical investigations of the crustal thickness and structure in southern Kamchatka (Baboshina et al., 2000; Geological Map of the Russian Federation, 2000) reveal the presence of reworked continental crust that is 38–40 km thick (**Figure 2**). A wide spectrum of zircon ages going back to 3.4 Ga (Hourigan et al., 2009; Bindeman et al., 2016) indicates metamorphosed mixed siliceous sediment origin. A magnetotelluric profile conducted along the line from Opala volcano to the northwest (line I-I' on **Figure 2**) cross-cuts the Karymshina Caldera just to the north of its center (**Figure 3**). It revealed locally thickened gabbroic lower crust and thinned upper crust, as well as increased thickness of volcanic rocks and volcaniclastic Cenozoic sediments. Although not interpreted by the original authors to reflect the magmatic evolution of KVC, we below interpret this structure as an indication of substitution of the upper crust by a massive series of basaltic sills leading to the "basaltification" of the mid to upper crust via mantle-derived intrusions.

The large-volume rhyolitic eruption at Karymshina at 1.78 Ma represents an unusual and rare event for volcanic arcs, as single caldera-forming eruptions with volumes in excess of 100 km^3 are all but unknown in most volcanic arc segments around the world (de Silva, 2008). Eruptions on this "supervolcanic" scale are instead confined to "flareups" of magmatism which represent events in some continental arcs characterized by extremely rapid production of silicic volcanic rocks and intrusions over a relatively short period of as little as a few Myr (de Silva et al., 2006; Ducea and Barton, 2007; Ducea et al., 2015a,b). These flareups, also referred to as high-volume magmatic events (Ducea et al., 2015a), can be responsible for producing as much as 90% of the granitoid intrusions in a continental arc such as the Sierra Nevada in the western United States (Ducea et al., 2015a). The origin of these flareup events remains controversial, with various authors proposing the underthrusting of fertile upper crust in a compressive tectonic regime to depths suitable for voluminous melting (Ducea and Barton, 2007; DeCelles et al., 2009), a thermal runaway where steady intrusion of basalt produces a

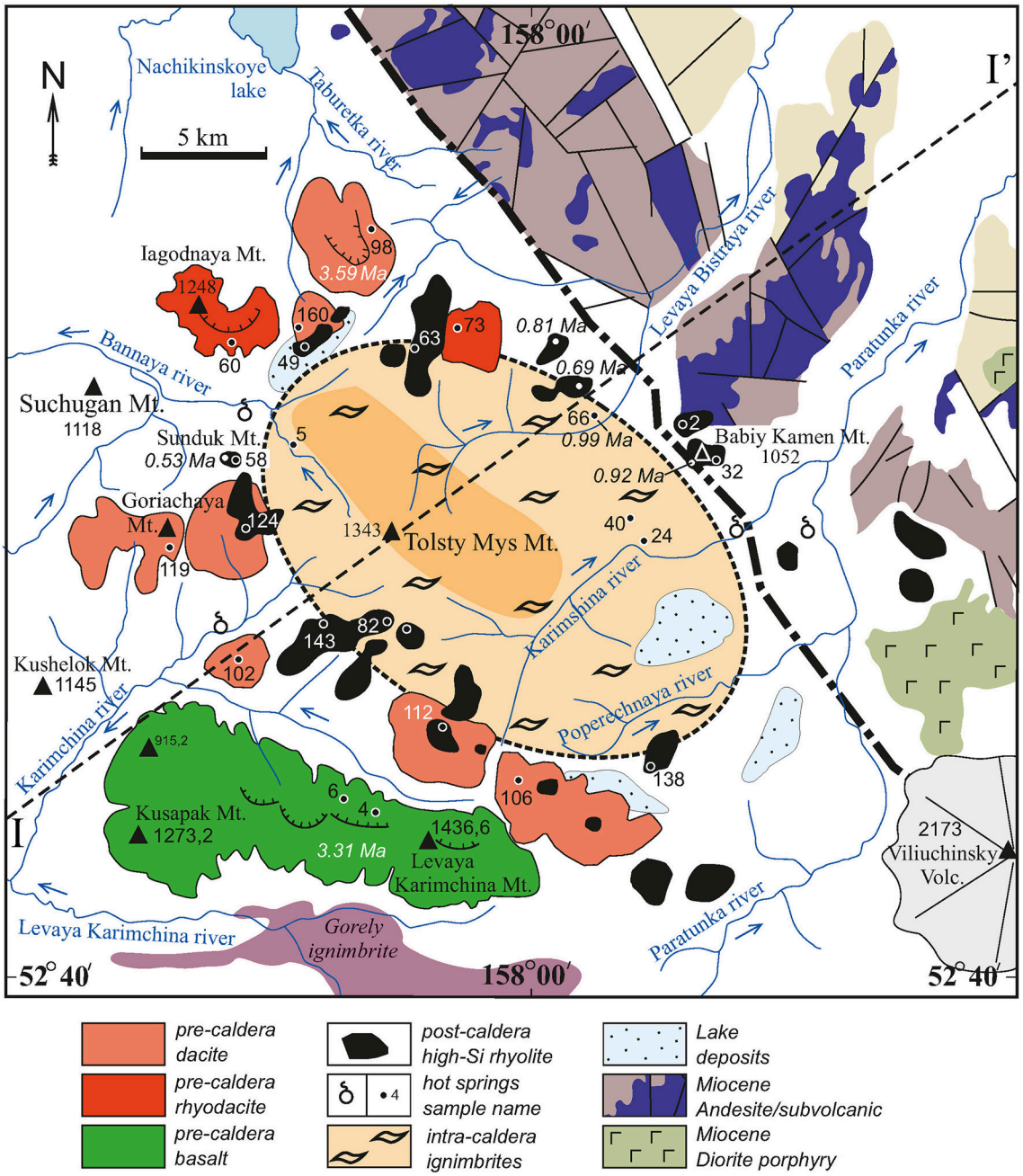

FIGURE 2 | A geologic map of Karymshina Volcanic Complex showing topographic features, inferred 1.78 Ma Karymshina caldera boundary (dashed line), pre- and post-caldera extrusive domes and volcanoes. Numbers represent ages from this study (**Table 2**) and compiled from the literature (**Table 1**). The last two-three digits of sample names from this study (e.g., 119 is 119L-2005) corresponds to the **Table 1**. The area of the caldera contains several ignimbrite sheets, which reach visible thicknesses of 1,000 m on the eastern edge and contain no observable stratigraphic compositional differences (**Table A1**). These ignimbrite sheets wedge out as they approach the edges of the depression near the volcanoes Goryachaya, Yagodnaya, and Sunduk. The volcanic products of those volcanoes and additional large extrusions overlay the ignimbrite sheets along the supposed ring fracture. Miocene porphyries include granodiorites from 11 to 14 Ma Zavoikovsky complex and 11.4 Ma Akhomten granitic complex is to the southeast (**Figure 1**). Dashed line I and I′ represent geophysical profile from Geological Map of the Russian Federation (2000) shown on **Figure 3**.

highly non-linear increase in the amount of crustal melting above a certain threshold (Dufek and Bergantz, 2005; Karakas et al., 2017), or a sudden increase in melting in the mantle wedge due to either rollback of the overriding slab (DeCelles et al., 2009) or the delamination of the dense mafic lowermost crust and mantle lithosphere, leading to sudden decompression

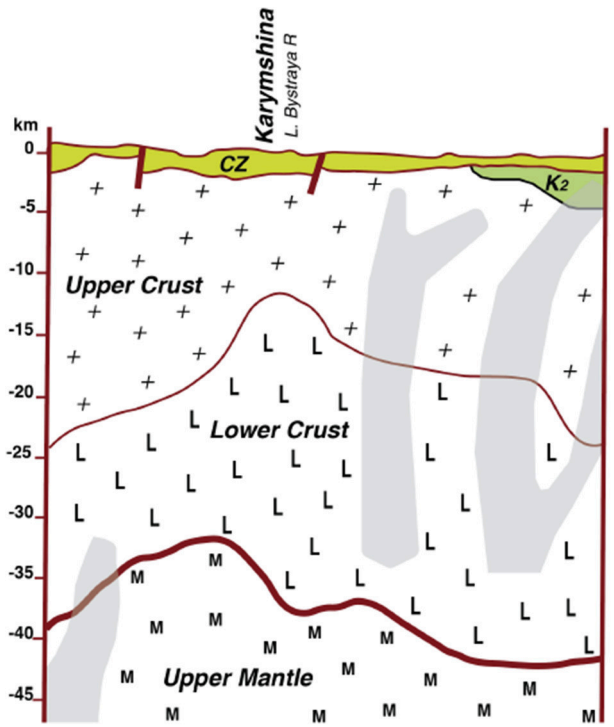

FIGURE 3 | Seismic profile across Karymshina caldera (Geological Map of the Russian Federation, 2000) showing regional 38–40 km thick continental crust and crustal structure. Notice thinned upper crust and locally thickened lower crust under Karymshina that we interpret here as representing basaltic sills that were added to the upper crust causing its partial melting and progressive substitution with more mafic residue and basaltic cumulate in the process of magmatic evolution of Karymshina Volcanic Complex. CZ is Cenozoic volcanic and volcaniclastic cover, K_2 is Upper Cretaceous crust. Vertical gray areas represent faults according to magnetotelluric seismic imaging.

melting of the mantle (de Silva et al., 2006; Lee et al., 2006). DeCelles et al. (2009) argue against this latter model, pointing out that magmas associated with flareups tend to have lower ε_{Nd} values, indicating that crustal melting was disproportionately responsible for producing the silicic intrusions relative to the differentiation of a greater volume of mantle-derived basalts. However, Colón et al. (2018a) pointed out that greater magmatic fluxes from the mantle actually serve to increase the proportion of crustal melt in the resulting rhyolites, as the greater heat allows more crust to melt at a slightly faster rate than it allows for more basalts to be differentiated to rhyolite, a result which we replicate here.

In this study, we summarize data obtained in the past decade and provide geological, mineralogical, whole rock major and trace element characterization of the caldera-forming ignimbrites, and newly described pre- and post-caldera extrusions and ignimbrites, and present results of new geochronology and analysis of O, Sr, Nd, and H isotopes in the eruptive products. We supplement this information with the results of rhyolite-MELTS modeling of crystallization and assimilation, and results from thermomechanical modeling of magma genesis in the unusually voluminous Karymshina system.

METHODS

Mineralogy and Petrography

Thin sections of five samples of the top (36L-2007) and middle-bottom (samples 24L-2006, 40L-2007) of the ignimbrites and postcaldera intrusions (samples 2L-2008, and 58L-2006 in **Table 1**) were analyzed by electron microprobe (**Table A3**, **Figure 4**). An additional three covered thin sections (5G-2005, zh356, and zh423) were used for crystal abundance counting on a petrographic microscope (**Table A1**).

Electron microprobe analyses were performed at Lokey Laboratories at the University of Oregon on a Cameca SX-100 using an accelerating voltage of 15 kV, a 30 nA beam current, and a 10 μm spot beam size. Several plagioclase crystals were analyzed from each sample, as well as some amphiboles, plagioclase crystals within autholithic xenocrysts, and the glass matrix. Three spot analyses were used to classify plagioclase zoning types: normal and reverse concentric, complex, and unzoned. Cores were also analyzed for xenolith-hosted plagioclase. Amphiboles were chosen due to the existence of exsolution rims. Spot analyses of the amphiboles were performed at the core and within the exsolution rims. Glass matrix was analyzed in several locations to check for potential variations. Whole rock major and trace element analyses were performed by XRF using fused Li-Borate discs at Washington State University.

Trace element concentrations were determined by LA-ICP-MS at Oregon State University on matrix glass from ignimbrite samples as well as tephras selected in selected North Pacific IODP drill sites from sediment intervals matching the age of major Kamchatkan ignimbrites. Analytical procedures generally followed Loewen and Kent (2012) using a Photon Machines 193 nm ArF laser coupled to a ThermoScientific X-Series ICP-MS. A 50 μm spot at 7 Hz was used to ablate glass ± epoxy. Blank analyses of epoxy verified that no significant trace element signature was present. Silica from electron microprobe analyses done on the same or similar samples or similar samples was used for an internal standard, and analyses were calibrated with GSE-1G. Results are presented in **Table A2**.

Isotope Geochemistry

Oxygen isotopes were analyzed in plagioclase and quartz using samples weighing ∼1.5 mg by CO_2 laser fluorination and the MAT 253 gas source mass spectrometer at the University of Oregon. All analyzed crystals were visually checked under the microscope to ensure they were free of visible inclusions and lacked visible alteration due to weathering. The largest phenocrysts were analyzed individually (**Table 3**) and several crystals were analyzed per sample to check for isotopic variation among the phenocrysts. However, none was found and thus bulk analyses are robust. Two samples of zircon from the top and the bottom of Karymshina ignimbrites 2006L-24 and 2007L-36 were analyzed at the UCLA ion microprobe facility on the Cameca 1270 ion microprobe using a Cs primary beam and polished zircon mounts used previously for U-Pb dating, and the data was presented in Bindeman et al. (2010) and Bindeman and Simakin (2014).

TABLE 1 | Description of samples from Karymshina Volcanic Complex used in this study.

Sample ID	Latitude	Longitude	location/name	Age, Ma	Comment	Minerals, %
PRE-CALDERA EXTRUSIONS						
6L-2010	N 52.725990°	E 157.900490°	Basalt volcano, S edge of caldera			
4L-2010	N 52.721800°	E 157.921780°	Basalt volcano, S edge of caldera	3.312 ± 0.078		
160L-2008	N 52.889056°	E 157.867356°	Small dacite volcano, cut by caldera rim			
102L-2008	N 52.776229°	E 157.839537°	Small dacite volcano, cut by caldera rim			
73L-2011	N 52.888304°	E 157.962367°	Dacite volcano, N rim of caldera			
60L-2004	N 52.883933°	E 157.838324°	Dacite volcano on the rim, NW from it			
98L-2008	N 52.925247°	E 157.911999°	Dacite volcano, rim of caldera	3.586 ± 0.006		
106L-2006	N 52.737887°	E 157.990413°	Dacite volcano, S rim of caldera, ignimbrite are overlying it			
119L-2005	N 52.814119°	E 157.823909°	Dacite volcano, Goryachaya Mt, W of caldera, part of volcano is burried by ignimbrites			
KARYMSHINA IGNIMBRITES						
36L-2007	N 52.835347°	E 158.066208°			*	Pl19%Qz20%Gl46%
37L-2007	N 52.834460°	E 158.066177°	”		*	
38L-2007	N 52.833834°	E 158.065502°	”		*	
39L-2007	N 52.831718°	E 158.064906°	”		*	
40L-2007	N 52.829532°	E 158.065741°	”	1.78 ± 0.02	*	
41L-2007	N 52.827850°	E 158.071454°	”		*	
24L-2006	N 52.818792°	E 158.084820°	”	1.78 ± 0.02	*	Pl25%Qz21%Gl42%
43L-2007	N 52.825947°	E 158.079612°	”		*	
44L-2007	N 52.825029°	E 158.080838°	”		*	
45L-2007	N 52.823854°	E 158.082877°	”		*	
46L-2007	N 52.823223°	E 158.083222°	”		*	
47L-2007	N 52.822530°	E 158.083612°	”		*	
321L-1972	N 52.617045°	E 158.318274°	Zhirovskaya ignimbrite		*	
5G-2005	N 52.846024°	E 157.866544°	Bannaya R Ignimbrite	1.388 ± 0.1	*	Pl46%Qz2%Gl53%
POST-CALDERA EXTRUSIONS						
107L-2005	N 52.886703°	E 157.795909°	Extrusion south of Yagodnaya Mt (older trakhirhyolite complex)			
124L-2005	N 52.818807°	E 157.844167°	Zubia Mt			
143L-2005	N 52.786572°	E 157.882363°	Height 1267.3m, upper R. Karymchina River			
49L-2006	N 52.880648°	E 157.868317°	Height 1047, R bank of Bannaya R			
45L-2004	N 52.843611°	E 157.824156°	Sunduk Mt	*0.53 ± 0.05*	=58L-06	
58L-2006	N 52.842885°	E 157.825792°				Pl23%Qz14Gl54%
63L-2005	N 52.880835°	E 157.929562°	Height 802m, Nachikinsky Creek		=75L-06	
112L-2006	N 52.746464°	E 157.949139°	Heigh 1439m, U Middle Karymchina R			
138L-2006	N 52.733089°	E 158.067444°	Plateau between Ovragia and Poperechnaya			
138L-2006	N 52.733089°	E 158.067444°				

(Continued)

TABLE 1 | Continued

Sample ID	Latitude	Longitude	location/name	Age, Ma	Comment	Minerals, %
80L-2007	N 52.784158°	E 157.921728°	Heigh 1269m, Upper R Karymchina R			
82L-2007	N 52.783616°	E 157.914261°	Height 1250, U R Karymchina R			
2L-2008	N 52.855487°	E 158.090884°	Height 973.8m next to Mt Baby Kamen	*0.5 ± 0.2*		Pl22%Qz17%Gl53%
32L-2007	N 52.840150°	E 158.106371°	Baby Kamen extrusion		0.919 ± 0.084#	*
35L-2007	N 52.840232°	E 158.091856°	Post-Caldera extrusion/dike		*	
66L-2013	N 52.866948	E 158.022530	Intra-caldera ignimbrite	0.988 ± 0.026	*	
PRE CALDERA IGNIMBRITES						
10L-2015	N 52.833937	E 157.208486	Extra-caldera ignimbrite		3.77 ± 0.002	
13L-2015	N 52.745852	E 157.390212	Extra-caldera ignimbrite		3.853 ± 0.022	
89L-2013	N 52.877498	E 157.593793	Extra-caldera ignimbrite		3.622 ± 0.039	
77L-2016_2	N 52.905098	E 157.929458	Q-Bi tuff		3.839 ± 0.029	
139L-2013	N 52.925439	E 157.530176	Extra-caldera ignimbrite		3.634 ± 0.071	
111L-2010	N 52.510582°	E 158.214476°	Karymshina-Zhirovskoy, Falshivaya River 100m under powed station, 4Ma	4.11 ± 0.09#	**	

**Published in Bindeman et al. (2010), **age published in Seligman et al. (2014); Italics - published Ar Ar ages from Sheimovich. # zircon U-Pb age; =sample number is for identical sample.*

Hydrogen isotopes were analyzed in biotite and amphibole using samples weighing ∼1.5 mg on the high temperature conversion/elemental analyzer (TC/EA) coupled with the MAT 253 mass spectrometer at the University of Oregon. Only biotite and amphibole samples from the ignimbrites were microscopically fresh and were analyzed for D/H; lesser and commonly insufficient quantities of these minerals are present in postcaldera intrusions and they are additionally display greater alteration into chlorite. Analyzed 1.5 mg of samples were visually checked for the absence of chloritization or oxidation. Data were normalized relative to new USGS standards 57 and 58 on a SMOW scale (Qi et al., 2017).

Whole rock $^{86}Sr/^{87}Sr$ and $^{144}Nd/^{143}Nd$ ratios were analyzed at the New Mexico State University by Dr. Frank Ramos using standard column chemistry and TIMS VG Vector 54 instrument.

$^{40}Ar/^{39}Ar$ analyses were performed at the WiscAr laboratory at the University of Wisconsin-Madison. All $^{40}Ar/^{39}Ar$ dates are calculated relative to the 28.201 Ma Fish Canyon sanidine standard or the 1.1864 Ma Alder Creek sanidine standard (Jicha et al., 2016) using the decay constants of Min et al. (2000). Complete analytical methods and data are provided in the online supplement.

Magmatic-Thermomechanical Modeling

To further investigate the origins of the huge volumes of magma produced in a relatively short time at Karymshina, we used a slight modification of the 2D model used for the Yellowstone hotspot in Colón et al. (2018a), which is in turn a modification of the original large scale thermomechanical code developed by Gerya and Yuen (2003). The model setup that we use for Kamchatka, where the crust is 30–38 km thick (**Figures 1**, **2**) is identical to what is described in the Colón et al. (2018a) study, with a few key exceptions. We retain the use of a mantle plume to produce melts which fuel volcanism, instead of using a fully realized model of a dehydrating subducting slab, a choice which we justify in light of the fact that we are primarily interested in processes in the top ∼70 km of the crust and upper mantle, rendering the actual source of mantle melting less important, and avoiding for now the complicated task of setting up a realistic subduction geometry. Unlike in the Colón et al. (2018a) model, the lithosphere is fixed relative to the ascending plume, and the plume is much cooler and weaker than in the Yellowstone model, to more accurately reproduce a typical subduction flux for the arc (e.g., Jicha and Jagoutz, 2015). The plume advects from the base of the model at a rate of ∼3,700 km^2/Myr, as in Colón et al. (2018a), but has a much lower potential temperature of 1,475°C (compared to a background value of 1,350°C) to produce the desired amount of mantle melting. We also begin the model with only a 50 km thick lithosphere (compared to 80 km for the Yellowstone study). Further modifications from the code of Colón et al. (2018a) include higher melt fractions for basalts at given temperatures and pressures, to account for the much higher water contents of subduction zone magmas, and minor improvements to the way melt is transported in the crust (these changes described in Colón et al., 2018b).

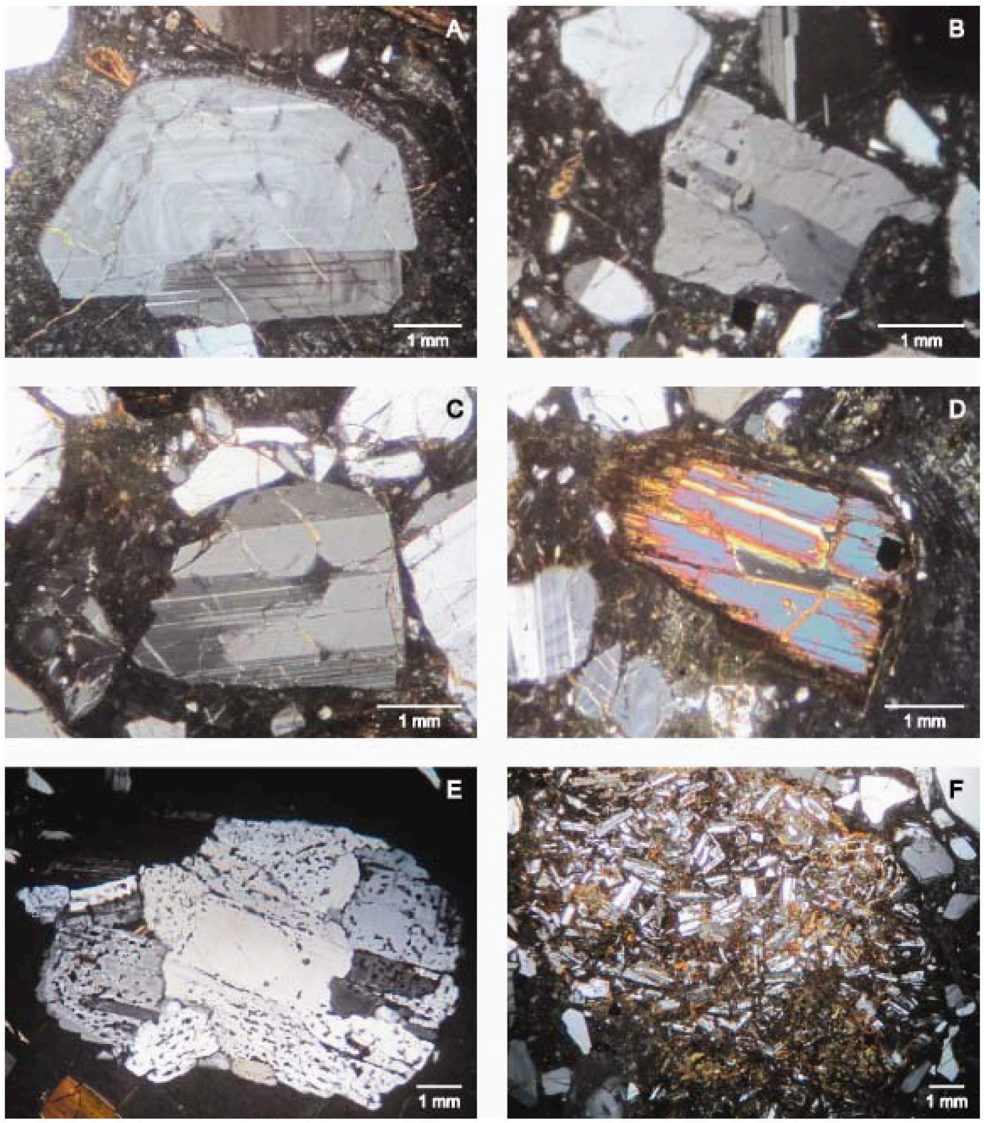

FIGURE 4 | Thin section mineralogy of 1.78 Ma ignimbtite from Karymshina caldera (samples 40L-2007 and 36L-2007). Plagioclase phenocrysts exhibit **(A)** concentric zoning, **(B)** complex zoning, and **(C)** no zoning. Other features present in the Karymshina samples are **(D)** amphibole phenocrysts with reaction rims, **(E)** agglomerations of plagioclase crystals, some with sieve texture, and **(F)** autolithic xenoliths which include small phenocrysts of plagioclase.

RESULTS

Geologic Position and Geochronology of the KVC

The Karymshina Volcanic Complex is located on the active eastern volcanic front of Kamchatka Peninsula, ∼50 km southwest of the regional capital city of Petropavlovsk-Kamchatsky (**Figures 1**, **2**). Our new map of the KVC, shown on **Figure 2**, is a result of a decade-long geologic, geochronologic, and geochemical investigation. It demonstrates that the KVC is made of 4.1–0.5 Ma predominantly silicic rocks represented by thick tuff units and pre- and postcaldera extrusions and volcanoes. The area surrounding Karymshina Caldera includes several hot springs (**Figure 2**) suggesting a source of heat from recent magmatic activity younger than synvolcanic 0.5 Ma intrusions at depth. For example, the 300 × 500 m Bannaya River geothermal field in the NW part of ring fracture (**Figure 2**) was mapped in 1976 and is active today with temperatures exceeding 90°C in several places (Kraevoi et al., 1976; Rogozin et al., 2015). Below we describe the geologic position of the KVC based on analysis of regional geology and our new observations.

Subduction Parameters and Basement and Country Rocks

The depth to the subducting plate under KVC is 140 km (Gorbatov et al., 1999, 2001; Baboshina et al., 2000; Nizkous et al., 2007); 110–140 km is a relatively typical configuration for Eastern Volcanic Front volcanoes, including the younger

Gorely caldera directly to the south (Seligman et al., 2014). Seismic data on the crustal structure directly across the KVC (Geological Map of the Russian Federation, 2000, Explanations, **Figure 3**) shows that the KVC has thinner (13–20 km) upper crust and a greater (2 km) thickness of the volcanic layer, an observation that we take below to indicate significant reworking of the whole crustal volume in the course of >4 Myr-long magmatism. Geologic units that immediately surround the caldera include the poorly studied middle Miocene South Bystinskaya volcaniclastic sediments of predominantly andesitic composition with ∼20 Ma K-Ar ages (**Figure 2**, Geological Map of the Russian Federation, 2000) that are uplifted and tectonized. These are coeval with subvolcanic dioritic, dioritic porphyritic, and granodioritic bodies of low-K, calc-alkaline affinity, with ages of 14–11.1 Ma (Zavoikovsky intrusive complex) around Vilyuchik volcano, immediately to the east of Karymshina (**Figure 2**).

Further east, the mid Miocene Akhomten granitic intrusive complex is exposed and ranges from intrusive facies ranging in composition from 60 wt% SiO_2 diorite to leucogranite with 76 wt% SiO_2. The U-Pb zircon age published by Seligman et al. (2014) for one of the units is 11.4 Ma, while previous K-Ar determinations range from 11 to 12.1 Ma in age (Vinogradov, 1995). Rocks of these granodioritic intrusions are petrographically comparable to the Karymshina volcanics and contain biotite and amphibole, with K-feldspar and quartz in the micropegmatoid groundmass. Rocks of Akhomten have also been studied for their whole rock Sr-Nd and O isotopes (Vinogradov et al., 1986; Vinogradov, 1995) and display a diverse range of $^{87}Sr/^{86}Sr$ values (0.7034–0.7036), which are on the high end of younger rocks in the area (Vinogradov et al., 1986). $^{143}Nd/^{144}Nd$ ratios are characteristic of typical mantle (0.51305–0.51325, ε_{Nd} is +3 to +9), while low $\delta^{18}O$ values go down to −3% indicate that this shallow subvolcanic intrusion underwent significant hydrothermal alteration by meteoric waters during emplacement and cooling. Older Cretaceous rocks, also arc derived, are not exposed in the immediate area but are found in greenschist facies volcanics and sediments to the east, around the city of Petropavlovsk (**Figure 1**), and in the uplifted amphibolitic Ganal complex ∼50 km to the north. Gabbro intrusions and detrital zircon in the Ganal amphibolites are 90–55 Ma in age and no older than the late Cretaceous, while metamorphic rims are ∼25 Ma in age (Bindeman et al., 2002) suggesting regional metamorphism was followed by rapid exhumation that brought granulite-grade rocks to the surface. Their Sr isotopes are diverse ($^{86}Sr/^{87}Sr$ from 0.703 to 0.706) and $^{143}Nd/^{144}Nd$ value extend to crustal values of 0.5124 (ε_{Nd} of −4.6; Vinogradov, 1995). These described regional rocks and their isotopic values represent potential source components for magmas in the KVC, used below for discussion of potential mechanisms of magma derivation.

Magmatic Rocks of the Karymshina Volcanic Complex

The thickest and most voluminous unit is represented by the 1.78 Ma rhyolitic intracaldera tuff, filling the area of the 25 × 15 km (**Figure 2,** thin section mineralogy—**Figure 4**). Its central part, Tolsty Mys Mt (1,343 m), is the highest in the area, and the source of several local rivers (**Figures 1**, **2**). Uplift of the Karymshina area as has led to the exposure of intracaldera tuff, obliteration of the topographic caldera expression, and erosion of most extracaldera tuffs except in the west (discovered recently and currently under investigation). Geological mapping in the area (Geological Map of the Russian Federation, 2000) and previous investigation by Sheimovich and Khatskin (1996) failed to identify the collapse caldera. Hundreds of meters of thick intracaldera ignimbrite sections mapped and studied by us across the Karymshina and Bannaya Rivers do not contain obvious mineralogical or compositional breaks (SiO_2 varies by is ∼1 wt% over 1,000 m, **Table A1**), and thus we interpret the section as a single intracaldera cooling unit from a single eruption, though this interpretation is not yet completely certain considering the incomplete nature of the outcrops. Additionally, Bindeman et al. (2010) dated the top and bottom of the 1,000 m thick intracaldera ignimbrite sheet by Ar-Ar and obtained identical ages of 1.78 ± 0.02 Ma. Previously reported U-Pb zircon ages (Bindeman et al., 2010) returned a single population of zircons overlapping within errors with ages 1.87 ± 0.11 Ma ($n = 9$, top ignimbrite) and 1.76 ± 0.09 Ma ($n = 8$, bottom ignimbrite), collectively overlapping within error with the 1.78 ± 0.02 Ma Ar-Ar biotite (eruption) ages for these samples in both cases. The similarity of the zircon crystallization ages to the eruption age indicates that zircon crystallization occurred immediately prior to the eruption, or within a short ∼20 kyr residence time given uncertainties. Cores of nine zircon in selected post-caldera extrusions near Babii Kamen also show no evidence of inheritance (Bindeman et al., 2010).

Using the dimensions of the caldera and the volume of intracaldera ignimbrites (275 km^3) given in Leonov and Rogozin (2007) it can be estimated that the total eruptive volume was about three times this number or close to 800 km^3 if ash and eroded extracaldera deposits are each 275 km^3 based on similar relationships proposed for the western USA calderas (Bacon, 1983). Lithic fragments in ignimbites and post caldera intrusions are represented by autholithic blobs consisting of elongated plagioclase in glass without quartz (**Figure 4F**) and silicified hydrothermally altered materials in quantities not exceeding a few percent. Below and in the **Table A2** we present analyses of the thickest ash layers in the Pacific corresponding to the 1.78 Ma nominal age of the eruption, in an attempt to find a Karymshina deposit there.

Two dozen post-caldera, high-silica rhyolitic extrusions have similar character outcrops and mineralogy but significantly higher silica contents than the ignimbrite. These extrusions form local topographic highs along the proposed caldera ring fractures of the 1.78 Ma caldera (**Figure 2**). Five are dated by us or previous researchers, and they are much younger than the Karymshina ignimbrite, ranging in age from 0.9 to 0.5 Ma. No volcanic rocks younger than ∼0.5 Ma have been dated and extrusive domes are eroded after uplift suggesting that the KVC is extinct, unlike neighboring active volcanoes.

Extracaldera ignimbrite layers that we tried to identify as correlative to the 1.78 Ma Karymshina ignimbrite instead returned ages both younger and older, and compositions that

are both more mafic and more silicic (samples 111L-2010, 4.11Ma, 2005G-5, 1.39Ma, **Table 1**). Pre-1.78 Ma dacitic to rhyolitic extrusions and basaltic volcanoes are exposed in the western and southern part of caldera, four of them dated in this study (**Tables 1**, **2**), returning ages of 3.62 and 3.84 Ma. A young dacitic tuff from the Bannaya River area was dated at 1.39 Ma (Bindeman et al., 2010), and is geochemically and isotopically distinct from the 1.78–0.5 Ma eruptive sequence. The quartz-biotite ignimbrites under the Zhirovskoy area near Gorely volcano returned older U-Pb zircon ages of 4.11–4 Ma, and similar tuffs are found in abundance in the western part of Karymshina caldera. These represent the oldest known volcanic units associated with the KVC. The above mentioned 11–14 Ma Akhomten and Zavoikovsky granitic and granodioritic complexes represent the latest dated silicic magmatism in the area before the ∼4.1 Ma onset of the voluminous silicic magmatism in the KVC.

The youngest volcanism in the region consists of the late Pleistocene-Holocene edifices of the surrounding volcanoes Vilyuchik, Gorely, and Mutnovsky, which are comprised by a differentiated series from basalts and basaltic-andesites to silicic domes unrelated to the KVC. The ∼0.5 Ma Zhirovskoy volcano Geological Map of the Russian Federation, 2000 and the voluminous 0.35–0.1 Ma dacitic to rhyodacitic voluminous ignimbrite sheets in the area are associated with caldera volcanism from the morphologically preserved Gorely caldera (**Figure 1**, Seligman et al., 2014) and are also not associated with the KVC, but we consider these products for comparison to the KVC. Given geochemical features, we consider the 1.39 Ma Bannaya River dacitic ignimbrites (2005G-5) exposed within the KVC to likely have originated outside of KVC, and by petrogenetic processes more similar to those at Gorely (Seligman et al., 2014).

Mineralogy and Petrography

Silicic rocks of both pre- and postcaldera rhyolitic lavas and ignimbrites in the KVC contain quartz, biotite, amphibole, plagioclase, and pyroxene, with accessory zircon and apatite (**Figure 4**), while sanidine is mostly absent in all but a few rocks (where it occurs as an interstitial phase), even in the relatively potassium-rich high-silica rhyolites. In contrast, many similar amphibole-biotite intraplate rhyolites with subduction signatures in western North America (e.g., the Fish Canyon and Bishop tuffs) with higher K_2O than the KVC contain sanidine as an abundant phenocryst in rhyolites of comparable SiO_2 content, as do Andean silicic volcanics (**Figure 5**) and many intraplate hotspot-related centers such as Yellowstone. Like Karymshina, neighboring basement granodiorites such as at Akhomten contain K-feldspar mostly in groundmass intergrown with quartz, suggesting that in Kamchatkan arc environments it appears only at near solidus temperatures.

Precaldera intrusions display a range of compositions (**Figure 5**) from basalts to rhyolites, and silicic rocks are also amphibole-bearing. High-K_2O varieties are found among them. The composition of the 1.78 Ma caldera-forming ignimbrites from several locations across the proposed caldera are quite similar, containing up to 40–45% of 0.5–1.5 mm phenocrysts of 16–21 vol% quartz, 19–25 vol% plagioclase, 0–4 vol% amphibole, 5–11 vol% biotite, and 1–3 vol% oxides with 42–48 vol% glass matrix (the rest are bubbles), with accessory zircon and apatite. Electron microprobe analyses are given in **Table A3**, Appendix. The Al-in hornblende barometer of Schmidt (1992) yields a 1.75–1.85 kbar equilibration pressure range for the 1.78 Ma Karymshina ignimbrite.

The ignimbrites examined in thin section and analyzed with the electron-microprobe display visible flow textures within the glass matrix and there appeared to be no alteration, except in the

TABLE 2 | Summary of $^{40}Ar/^{39}Ar$ ages of this study #.

Sample #	Description	Material analyzed	MSWD	$^{40}Ar/^{39}Ar$ age (Ma) ± 2 σ
4L-2010	Basalt volcano, S edge of caldera	Groundmass	1.05	3.31 ± 0.08
98L-2008	Dacite volcano, rim of caldera	Groundmass	1.18	3.59 ± 0.01
2007L-40*	Karymshina Ignimbrite	Biotite	0.51	1.78 ± 0.02
2006L-24*	Karymshina Ignimbrite	Biotite	0.44	1.78 ± 0.02
2005G-5*	Bannaya R Ignimbrite	Plagioclase	1.12	1.39 ± 0.10
10L-2010**	Ignimbrite, west of caldera	Feldspar	0.90	3.77 ± 0.00
66L-2013	Ignimbrite, L Bystraya	Plagioclase	0.97	0.99 ± 0.03
89L-2013**	Ignimbrite, west of caldera	Plagioclase	1.00	3.62 ± 0.04
139L-2013**	Ignimbrite, west of caldera	Plagioclase	1.14	3.63 ± 0.07
77L-2016_2**	Ignimbrite, west of caldera	Feldspar	0.85	3.84 ± 0.03
13L-2015	Ignimbrite, west of caldera	Feldspar	0.67	3.85 ± 0.02
Pau-1	Mt Orlinoye Krylo, pre-Pauzhetka	Groundmass	0.67	3.06 ± 0.12
707-6	Mt Klyuchevskaya, pre-Pauzhetka	Groundmass	0.71	2.88 ± 0.01
69L-2012	Stol Mt basalt	Groundmass	0.42	2.95 ± 0.03

Ages previously published in Bindeman et al. (2010).

***Ages calculated relative to 1.1864 Ma Alder Creek sanidine standard (Jicha et al., 2016).*

All other ages are calculated relative to 28.201 Ma Fish Canton standard sanidine standard (Kuiper et al., 2008).

Decay constants used are those of Min et al. (2000).

*#Analytical protocols for each analysis are provided in the **Appendix**, **Table A4** in Supplementary Material.*

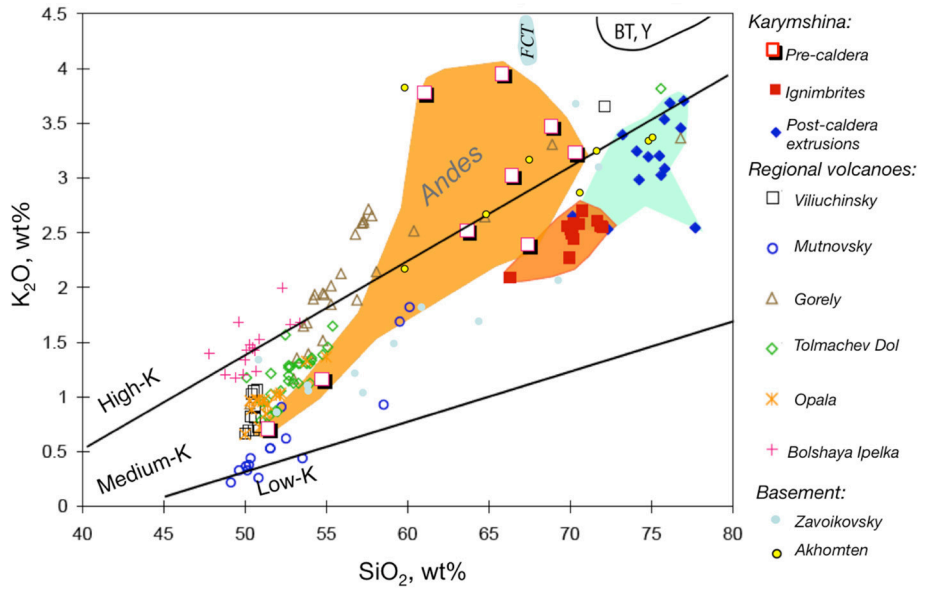

FIGURE 5 | K_2O-SiO_2 graph for Karymshina Volcanic Complex magmas and neighboring volcanoes. Central Andean magma compositional field is from Hildreth and Moorbath (1988). FCT, BT, and Y are ranges in the Fish Canyon tuff, Bishop tuff, and Yellowstone tuffs of western N America respectively, see **Figure 1** for caldera outline comparison.

case of the 1.39 Ma dacitic ignimbrite from the Bannaya River (2005G-5), which contained extensive radial textures indicating post-eruptive alteration of the sample and in which only 2% quartz by volume is present. In the majority of samples, larger phenocrysts of quartz contain hourglass melt inclusions and few phenocrysts of skeletal quartz. The larger phenocrysts also exhibited extensive microfracturing, common in an explosive eruption.

Plagioclase phenocrysts ranged from 19 to 23% by volume in most of the samples but is 46% by volume in sample 2005G-5. Often the larger phenocrysts were made of an aggregate of 3–4 individual crystals (**Figure 4**). Zoning patterns in the larger phenocrysts exhibited a wide range including concentric, normal, reverse, extremely complex (**Figure 4**). Microfracturing in plagioclase phenocrysts was also present, though not as prominently as in the quartz phenocrysts.

The ignimbrites also contain up to 5 vol% amphibole and biotite, almost all of them with reaction rims (**Figure 4D**). The opaque minerals (1–3 vol%) are primarily magnetite and ilmenite, with the presence of trace amounts of oxidation hematite as well. Magnetite-ilmenite thermometry gives a 700–750°C temperature range and an oxygen fugacity 0.25 log units above the NNO buffer. Other similar amphibole-biotite bearing rhyolites of Kamchatka such as the Dikii Greben volcano (Bindeman and Bailey, 1994) yield comparable to slightly more oxidizing f_{O2} buffer conditions (**Table A3**).

Groundmass in the 1.78 Ma Karymshina ignimbrite is variably crystallized and 16 spot analyses by electron microprobe yielded diverse spot to spot compositions, with many spots sensing sanidine crystals. The average of 16 spots in two ignimbrites is given in **Table A3** and has 74 wt% SiO_2 and 5 wt% K_2O.

Small antecrystic inclusions (**Figure 4F**), likely from an earlier episode of crystallization, perhaps from pieces cooled on the walls of the magma chamber contain 47–57 vol% glassy matrix and 43–49 vol% elongated plagioclase crystals. The rest of the inclusions are made of 0–4 vol% quartz, 0–3 vol% biotite, and 0–3 vol% opaque minerals.

The compositionally more evolved, high-silica rhyolitic post-caldera extrusions contain fewer phenocrysts: 22–24 vol% plagioclase, 14–17 vol% of quartz, 4–6 vol% of biotite, and 2–3 vol% of magnetite and ilmenite in a 53–54 vol% glassy and sometimes perlitic matrix. As with the ignimbrites, phenocrysts were often found in intergrown groups rather than individually. Melt inclusions were commonly present in the larger phenocrysts, in several phenocrysts creating a sieve texture. The larger phenocrysts exhibit a range of zoning from concentric to extremely complex. Both normal and reverse extinction patterns were observed. The larger phenocrysts also contained microfractures.

Deep Sea Sediment Record

Large caldera-forming eruptions from Kamchatka typically deposit ash into the north Pacific with dominant prevailing winds. Cao et al. (1995) and Prueher and Rea (2001) identified and stratigraphically dated 450 ash layers from IDDP sites 883 (N51.1983, E167.7688) and 882 (N50.3633, E167.600) ∼800 km southeast of Karymshina. We examined 5 of the thickest layers from the 1.6–1.9 Ma interval that could overlap with the 1.78 ± 0.02 Ma Karymshina ignimbrite age given analytical uncertainties and potential offset between stratigraphic and radiometric ages described in Ponomareva et al. (2018). For Hole 883, we studied intervals 7H6 (92–93 cm, 1.621 Ma, 10 cm-thick; 116–117 cm,

1.629 Ma, 8 cm-thick) and 8H-3 (128–129 cm, 1.902 Ma, 10 cm-thick). For Hole 882 we studied intervals 9H-1 (7.5–8.5 cm, 1.637 Ma, 10 cm-thick) and 9H-3 (35–36 cm, 1.728 Ma, 6 cm-thick).

Examined ash samples contained similar biotite-quartz-amphibole mineralogy as Karymshina ignimbrites. Electron microprobe major element and LA-ICP-MS trace element compositions are reported in **Table A2**. We also sampled ash intervals from 0.43 to 0.48 Ma looking for a match for the 0.44 Ma eruption at Pauzhetka (Bindeman et al., 2010) and the 0.35 Ma eruption from Gorely (Seligman et al., 2014), two calderas studied by us previously and available in the same drillholes.

Glass trace element ratios provide the most robust means to evaluate correlations between distal and proximal eruptive deposits—trace elements are more variable and thus provide a more unique compositional fingerprint than major elements, and ratios eliminate the need to use a major element internal standard in LA-ICP-MS analysis. In **Figure 12**, we visually compare our examined offshore ash layers to Karymhina ignimbrite glasses, none of which appear to compositionally overlap with the Karymshina deposit despite their similar ages.

Whole Rock Geochemistry

Table A1 presents new and compiled whole rock and microanalytical chemical analyses of pre- and postcaldera samples, a subset of samples across the 1,000 m-thick 1.78 Ma ignimbrite, and of a series of precaldera and postcaldera domes and ignimbrites. We additionally compiled a dataset for other Kamchatka and Karymshina-area volcanoes (Gorely, Mutnovsky, Opala, Akhomten Massif, and others) for comparison purposes, obtained from individual cited publications and from the GEOROC database. Additional data for the Zavoikovsky and Akhomten 14–11 Ma magmatic complexes was taken from Vinogradov (1995) and Geological Map of the Russian Federation (2000). Trends at the KVC fit the typical differentiation pattern for a metaluminous, medium K_2O magmatic series, spanning a large range from primitive basalts to more evolved rhyolitic magmas (**Figure 5**). New major and trace element data for the KVC shows that there is an overall increase over time in the level of differentiation and a decrease in chemical diversity from pre-caldera to caldera-forming and then to post-caldera extrusions (**Figure 5**, **Figure A1**). The latter represent the most differentiated and homogenous high-silica rhyolitic compositions with 75–77 wt% SiO_2 plotting on the highest end among Kamchatkan magmas, and in the highest known volumetric abundance of such magmas in one center, making it somewhat unique for Kamchatka. High-silica rhyolites have the highest concentrations of K_2O because none of the rocks contain phenocrysts of sanidine, which only occurs as an interstitial mineral in high-silica rhyolitic intrusions, and thus magmas are able to accumulate potassium and other incompatible trace elements in the most silicic differentiates. While high silica rhyolites are abundant in intraplate settings such as those found in the Western USA, they are generally uncommon in arcs (Winter, 2010). The main other occurrence of high silica rhyolites in arcs is the central Andes on top of an especially thick continental crust (**Figure 5**; Hildreth and Moorbath, 1988; de Silva and Gosnold, 2007; Folkes et al., 2011; Grocke et al., 2017).

As Kamchatka (as well as at the Kuriles and Japan) has a strong, many fold increase in K_2O with increasing distance from the trench (or depth to the subducting slab, Volynets, 1994; Duggen et al., 2007; Portnyagin et al., 2007; Kimura and Stern, 2008), the K_2O content of parental basalts or rocks at equal levels of differentiation but of different ages can be used to assess if subduction parameters changed over the duration of magmatism. Volcanic rocks from the KVC spanning 4 Ma plot in the typical mid-K level, between the forearc Mutnovsky and the back-arc Gorely and Tolmachev Dol volcanoes, a similar to other volcanoes of the Eastern Volcanic front. This suggest that the subduction parameters changed insignificantly for the last 4 Ma duration of magmatism. In particular, the 4 Ma quartz-biotite tuffs underneath the KVC largely overlap with the 1.78 Ma and later eruptive units. Additionally, the 14–11 Ma Zavoikovsky and Akhomten complexes and their intrusive equivalents which are proposed to serve as basement rock assimilants for Karymshina have largely overlapping K_2O-SiO_2 relationships.

Rb and Sr concentrations and their ratios put the Karymshina Caldera rocks (**Table A1**) within the typical arc-related I-type granitoids, indicating less differentiation of Rb with respect to Sr (Halliday et al., 1991; Anderson et al., 2000). Sr decreases with time from ∼350 to 150 ppm, while Rb stays consistently around 50–60 ppm, causing Rb/Sr ratios to increase from ∼0.1 to 0.4. The Karymshina caldera rocks appear to be typical of subduction zones under continental crust, coinciding with the Coastal Batholith in Peru and the Kosciousko Batholith (Halliday et al., 1991), consistent with plagioclase fractionation in the absence of sanidine.

Major and trace element profiles through the 1,000 m thick 1.78 Ma intracaldera ignimbrite (samples 2007-L-36 through 47 are listed in stratigraphic position top to bottom; **Table 1** and **Table A1**) show very little elemental variability, with the top ignimbrite tending to be a little more SiO_2 rich at 73 wt% vs. the 72 wt% at the bottom, with MgO, CaO, FeO concentrations, which are correspondingly lower by 0.2 wt%, and trace elements which are lower by 10 relative percent. This homogeneous intracaldera ignimbrite contrasts with the compositionally diverse precaldera lavas and domes. Postcaldera intrusions, despite their diverse ages, all consist of rather homogenous high silica rhyolite with 76–77 wt% silica.

Plotting KVC rocks as a time series with age groups from pre-caldera to caldera-forming to postcaldera (**Figure A1**), we observe a steady increase in SiO_2 that is accompanied by a decrease in compatible elemental concentrations of Y, Sr, Zr, P, Ti, V, Sc, Nd, Ga, Cu, and Zn, suggesting that amphibole, plagioclase, zircon, and apatite saturation and fractional removal can explain the trends for these elements. Besides silica, there is an insignificant and scattered increase in incompatible trace elements, including U, Rb, Ba, and K, as well as in trace elemental ratios such as Rb/Sr, Ba/Sr, K/Sr, and La/Y. Rb and Ba normally concentrate in sanidine with high partition coefficients and form strong trends in many magmas from the western USA such as the Bishop Tuff (Anderson et al., 2000), but these strong correlations are notably absent in Karymshina due to the lack of sanidine as

a fractionating phase. Scatter in these elements may also reflect mobilization by hydrothermal solutions. As we observed for major elements, temporal trends in many elements and ratios suggest a decrease in diversity of magmas with increasing youth, becoming more homogeneous as they also become more evolved.

Zirconium concentrations in whole rocks and computed saturation temperatures using the Watson and Harrison (1983) formulation show a slight decrease with time, and are relatively low for all rocks: from 804 ± 20°C for precaldera magmas, to 771 ± 12°C in the 1.78 Ma ignimbrites, to 779 ± 20°C in post caldera intrusions. Given the presence of amphibole and biotite in most magmas and crystal contents in 30–45% range, this agrees with the "cold and wet" magma definition pertinent to continental volcanic arcs (Miller et al., 2003; Loewen and Bindeman, 2016), and matches phase equilibria near-wet solidus conditions described for such systems worldwide, for example in Toba caldera in Indonesia (Chesner, 1998; Budd et al., 2017) or the intracontinental cold and wet Fish Canyon Tuff of the western United States (Bachmann and Bergantz, 2004), which has both oxygen isotopic and zircon saturation temperatures of 750°C.

Hydrogen Isotopes of Amphiboles and Biotites

Hydrogen isotope analyses (**Figure 6**) were only possible to obtain for fresh and cleaned amphibole and biotite crystals (several crystals amounting to ∼2 mg) in the rapidly quenched 1.78 Ma caldera-forming Karymshina ignimbrite as samples from the pre- and postcaldera extrusions were either too altered or lacked amphibole and biotite. As some amphibole crystals were surrounded by alteration rims (**Figure 4D**), we selected only the central parts of crystals for analysis. Biotites, due to their easier chloritization and exchange with recent rain and snow waters are considered as less reliable than amphiboles to record primary magmatic δD values (especially when analyses rely on many tens to hundreds of mg by conventional methods), though we only selected the freshest 1–2 mg. Values of δD ranged from −94 to −127% (SMOW) in biotites and from −105 to −133% in the two amphibole samples (44L-2007 and 47L-2007, respectively; **Figure 6**). The δD values obtained for both the biotites and the amphiboles are lighter than mantle-derived magmas and samples of other volcanic rocks from the Eastern Volcanic Field of Kamchatka studied by Taran et al. (1997), and if taken at face value represent some of the lowest measured δD values in Kamchatka. The H_2O contents in both the Karymshina samples and those from other volcanoes are similar and appropriate for fresh amphiboles and biotites, suggesting that this depletion is not due to chlorite alteration (a mineral with 12 wt% H_2O which easily exchanges with surface water). The large range of δD values, especially in biotites, likely reflects incipient exchange of D and H after intracaldera ignimbrite emplacement into the shallow crust with meteoric waters, and could also be due to post-eruption alteration of the cooling ignimbrite deposits (e.g., Hudak and Bindeman, 2008; Seligman et al., 2018). It is also possible that some of the low δD values are attributable to hydrothermal alteration of the magma source rock prior to genesis and eruption of the 1.78 Ma magma, and reflect lower-δD subglacial meteoric water values as glaciation in the northern hemisphere started at 2–2.6 Ma. Such hydrothermal alteration of the source rock would require assimilation of a shallow crustal source rock and would indicate the presence of a shallow magma chamber, consistent with the 1.8 kbar pressure estimate for the magma obtained with the Al-in hornblende barometer of Schmidt (1992). As hydrogen is a minor element in the crust compared to oxygen, assimilation of a small amounts of low-δD, low-$\delta^{18}O$ crust will significantly affect the δD of magma at much smaller assimilant to magma ratios than can change $\delta^{18}O$ (Taylor, 1986).

Oxygen Isotopes

Values of $\delta^{18}O$ in plagioclase and quartz phenocrysts are presented in **Table 3** and **Figure A2**, and define an overall normal magmatic range. The measured $\delta^{18}O_{Plag}$ and $\delta^{18}O_{Qz}$ values can be used to calculate the $\delta^{18}O$ values for the magma using the equations

$$\delta^{18}O_{magma} = \delta^{18}O_{qz} - 0.45 \quad (1)$$

$$\delta^{18}O_{magma} = 0.027(wt\%SiO_2) - 1.45 + \delta^{18}O_{plag} \quad (2)$$

with equation 1 being based on measurements in the Bishop Tuff and the wt% SiO_2 in equation 2 being that for the whole rock (Bindeman et al., 2004).

Pre-caldera basaltic volcanoes have $\delta^{18}O$ values of 6.6–6.7% that are ∼1% higher than normal mantle-derived basalts (**Figures 7**, **8**). The overall high-$\delta^{18}O$ values in many basalts from Kamchatka are explained by assimilation of high-$\delta^{18}O$, lower crustal amphibolitic sources, such as those exposed in the Ganal Massif (**Figure 1**, Vinogradov, 1995; Bindeman et al., 2004, 2010). The 4.1 Ma quartz-biotite tuffs (e.g., 111L-10) with a $\delta^{18}O$ value of 6.75% can be explained by simple fractional crystallization of mantle-derived basalt, while a small precaldera dacite volcano (73L-111) has slightly depleted $\delta^{18}O$ values of 5.35%, requiring some low-$\delta^{18}O$ rocks in its genesis. This modest heterogeneity in precaldera $\delta^{18}O$ values contrasts with overall higher $\delta^{18}O$ values and greater homogeneity of the voluminous 1.78 Ma ignimbrite with $\delta^{18}O_{Plag}$ of 5.71–6.53 % and $\delta^{18}O_{Qz}$ of 7.3–7.9%. $\delta^{18}O$ homogeneity further increases in the high-silica rhyolitic, post-caldera extrusions with $\delta^{18}O_{Plag}$ of 6.22–6.55% and $\delta^{18}O_{Qz}$ of 7.1–7.55% despite their >1 Myr span in their ages. The mean of pre-caldera, caldera-forming, and post-caldera eruptive products have computed $\delta^{18}O_{Melt}$ values of 6.8 ± 0.6% (1 s.d.), 6.65 ± 0.4% and 6.85 ± 0.1%, respectively, suggesting comparable values averaged from diverse-in-$\delta^{18}O$ source rocks (**Table 3**). This overall normal range for silicic rocks in the KVC lacks the major depletions in $\delta^{18}O$ explained by the melting and assimilation of hydrothermally altered intracaldera rocks which occur in the neighboring Gorely volcano (Seligman et al., 2014) and in many other Kamchatkan calderas (Bindeman et al., 2004, 2010). The 6.7–6.9% values of the KVC are similar to slightly higher than what would be expected for magmas derived by pure fractional crystallization of a 5.7% MORB source (Bindeman et al., 2004), but slightly lower in $\delta^{18}O$ than a differentiation product of the above-mentioned high-$\delta^{18}O$ basaltic pre-caldera

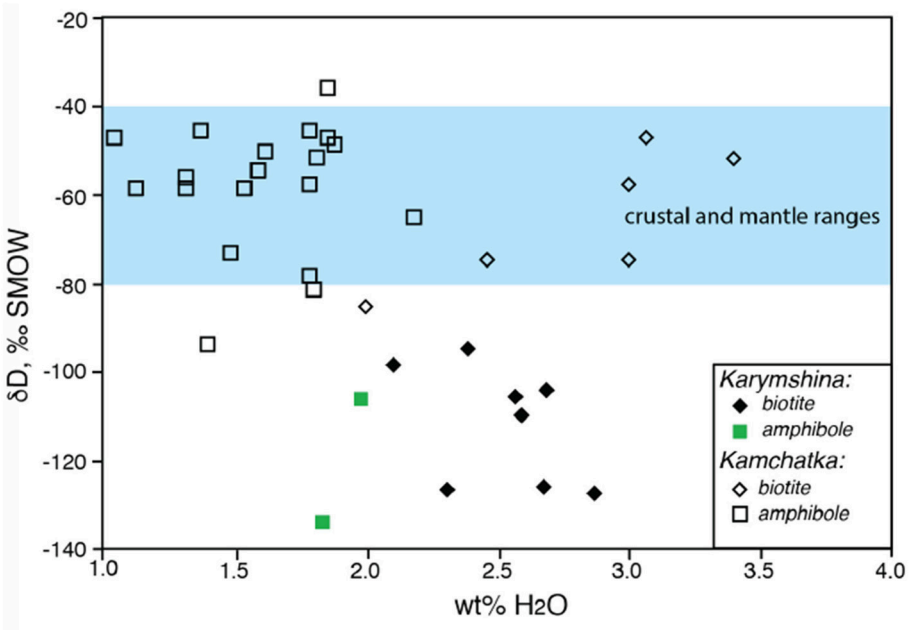

FIGURE 6 | δD and H_2O in Karymshina biotites and amphiboles in comparison to other published data for Kamchatka (Taran et al., 1997; Shipley, 2011). Notice lower δD range for Karymshina magmas but comparable H_2O content suggesting lack of significant chloritization of analyzed minerals. Overall low-δD values (lower than typical crustal and mantle values) would agree with assimilation of hydrothermally-altered rocks, possibly altered by low δD and low $\delta^{18}O$ meteoric waters during Pleistocene glaciation.

volcanoes (4L- and 6L-2010) which have $\delta^{18}O$ values of 6.7%. Pure fractional crystallization of these compositions should yield a ∼0.4–0.5% higher silicic differentiation product, with $\delta^{18}O_{melt}$ >7.2%, values rare at KVC. Avoiding these compositions requires the incorporation of some small amount of lower $\delta^{18}O$ hydrothermally altered crustal rock into the higher-$\delta^{18}O$ magma, a process easily justifiable, given the current hydrothermal activity in the area (Bindeman et al., 2004, 2010). A range in $\delta^{18}O$ values from higher-$\delta^{18}O$ amphibolite to lower-$\delta^{18}O$ high silica hydrothermal sinters was used as assimilants in the rhyolite melts models by Shipley (2011) and discussed later in this paper. Further evidence supporting the involvement of rocks hydrothermally altered by low-$\delta^{18}O$ and low-δD meteoric waters in the petrogenesis of the KVC additionally comes from: (i) low-δD values of amphiboles (**Figure 5**) and (ii) heterogeneity of $\delta^{18}O$ values and the presence of low-$\delta^{18}O$ zircon phenocrysts in the 1.78 Ma caldera-forming Karymshina ignimbrite (reported in Bindeman and Simakin, 2014), where zircon shows some modest heterogeneity of $\delta^{18}O$ values from 6.1 ± 0.3% to 4.7 ± 0.3%, with one crystal at 4.2 ± 0.3% (quoted ± are analytical 1 s.d. of ion microprobe analyses based on standards). These authors interpreted zircon diversity as reflecting assembly of diverse-in-$\delta^{18}O$ magma batches in petrogenesis of the Karymshina ignimbrite. Such processes are much more prominent in hot and dry intraplate low-$\delta^{18}O$ rhyolites elsewhere in the world, and are somewhat more muted in cold and wet arc magmas such as the Fish Canyon and Toba Tuffs (Bindeman and Simakin, 2014; Colón et al., 2015, 2018c; Budd et al., 2017).

$^{87}Sr/^{86}Sr$ and $^{143}Nd/^{144}Nd$ Isotope Ratios

$^{87}Sr/^{86}Sr$ ratios in whole rock samples of caldera-forming ignimbrites range from 0.7033 to 0.7035, while ε_{Nd} values range from +6.3 to +13.2 (**Table 3**), indicative of a predominance of depleted mantle-derived material within the magma (**Figures 7**, **8**). The range of values overlaps with isotopic compositions for neighboring Late Pleistocene-Holocene volcanoes and other volcanoes from the Eastern Volcanic Zone of Kamchatka (Hawkesworth et al., 1997; Churikova et al., 2001; Duggen et al., 2007; Seligman et al., 2014; Simon et al., 2014), with the surprising exception of very radiogenic Nd isotopes in three studied post-caldera high-silica rhyolitic intrusions that have ε_{Nd} values of +11 to +13 (**Table 3**, **Figures 7**, **8**), the highest in the region. These ratios suggest that no high-$^{87}Sr/^{86}Sr$ and low-ε_{Nd} reworked Precambrian crust or its associated sediments, such as is found in the Sredinny Range, played a role in magma genesis. Instead, Cretaceous and younger mafic basement crust such as the nearby Ganal amphibolites as well as granites similar to the 11 Ma Akhomten Massif found to the east (**Figure 2**) do serve as possible assimilants with $^{87}Sr/^{86}Sr$ ratios approaching 0.706 (Vinogradov, 1995; Seligman et al., 2014). Thus, the crustal melting required by the $\delta^{18}O$ and δD values which indicate that some crustal component must have been present and undergone hydrothermal alteration and recycling, must consist of predominantly young material.

When plotted as a time series, $^{87}Sr/^{86}Sr(i)$ isotopic ratios corrected for age using measured Rb/Sr ratios decrease, while ε_{Nd} values increase with time (**Figure 8**), demonstrating an increase

TABLE 3 | Isotope analyses of Karymshina Volcanic Complex samples.

Sample ID	SiO_2	K_2O	δ18O Plag	δ18O Qz Quartz	δ18O Melt*	87Sr/86Sr i	143Nd/144Nd	ε_{Nd}
PRE-CALDERA EXTRUSIONS								
6L-2010	54.72	1.16	6.7		6.73	0.70335	0.513026	7.6
4L-2010	51.37	0.71	6.62		6.56			
160L-2008	65.79	3.95	5.71		6.04			
102L-2008	63.61	2.52	6.18		6.45			
73L-2011	70.28	3.23	5.35		5.80	0.70343	0.51305	8.0
60L-2004	68.81	3.47	6.4		6.81	0.70350	0.51299	6.9
98L-2008	62.56	3.88	7.48		7.68	0.70353	0.512962	6.3
106L-2006	67.37	2.39	6.49		6.86			
119L-2005	66.38	3.02	6.22		6.56	0.70345	0.513027	7.6
KARYMSHINA IGNIMBRITES								
36L-2007	70.55	2.55	6.53		7.06	0.70331	0.513065	8.3
37L-2007	69.78	2.56						
38L-2007	71.64	2.61						
39L-2007	71.86	2.56						
40L-2007	70.78	2.56	6.33	7.91	7.13	0.70330	0.513048	8.0
41L-2007	70.00	2.53						
24L-2006	70.29	2.58	5.71	7.26; 7.50	6.66			
43L-2007	70.20	2.59						
44L-2007	70.19	2.44						
45L-2007	70.71	2.70						
46L-2007	70.10	2.49						
47L-2007	69.95	2.27		7.75	7.54			
321L-1972	66.01	2.51		7.72	7.42	0.70331	0.513015	7.4
5G-2005	62.91	2.09	5.9; 5.76	4.09(Px)	5.98	0.70332	0.513048	8.0
POST-CALDERA EXTRUSIONS								
107L-2005				7.22	6.77			
124L-2005	74.23	2.98	6.38	7.37	6.93			
143L-2005	76.54	3.96		7.31	6.89	0.703454	0.513326	13.4
49L-2006	70.80	4.30	6.22					
45L-2004	73.01	3.81	6.36	7.08	6.63	0.703312	0.513209	11.1
58L-2006	75.01	4.06						
63L-2005	75.82	3.08	6.39	7.55	7.10			
112L-2006	76.98	3.70	6.34	7.14	6.69			
112L-2006	76.98	3.70	6.49	7.3	6.98			
138L-2006	72.32	2.53	6.51	7.56	7.06			
138L-2006	72.06	4.08						
80L-2007	75.60	3.02	6.33	7.23	6.85			
82L-2007	75.80	3.53	6.56	7.43	7.07			
2L-2008	74.59	4.12	6.36	7.16	6.71	0.703317	0.513199	10.9
32L-2007	77.40	3.20						
35L-2007	73.22	3.39						
66L-2013	72.30	2.74		7.16	6.71			
PRE CALDERA IGNIMBRITES								
10L-2015	71.99	3.55						
13L-2015	70.74	3.22						
89L-2013	72.40	3.23		6.63				
77L-2016	73.00	3.33						
139L-2013	70.18	3.22						
111L-2010	69.07	2.41		6.77	6.32	0.70356	0.51321	11.2

*Sr isotopes are corrected for erution age using Rb and Sr concentrations; underlined is incorrected for age, but likely be 0.7034XX if likely 0.5–1 Ma age is used. *Melt is computed using minerals (see text).*

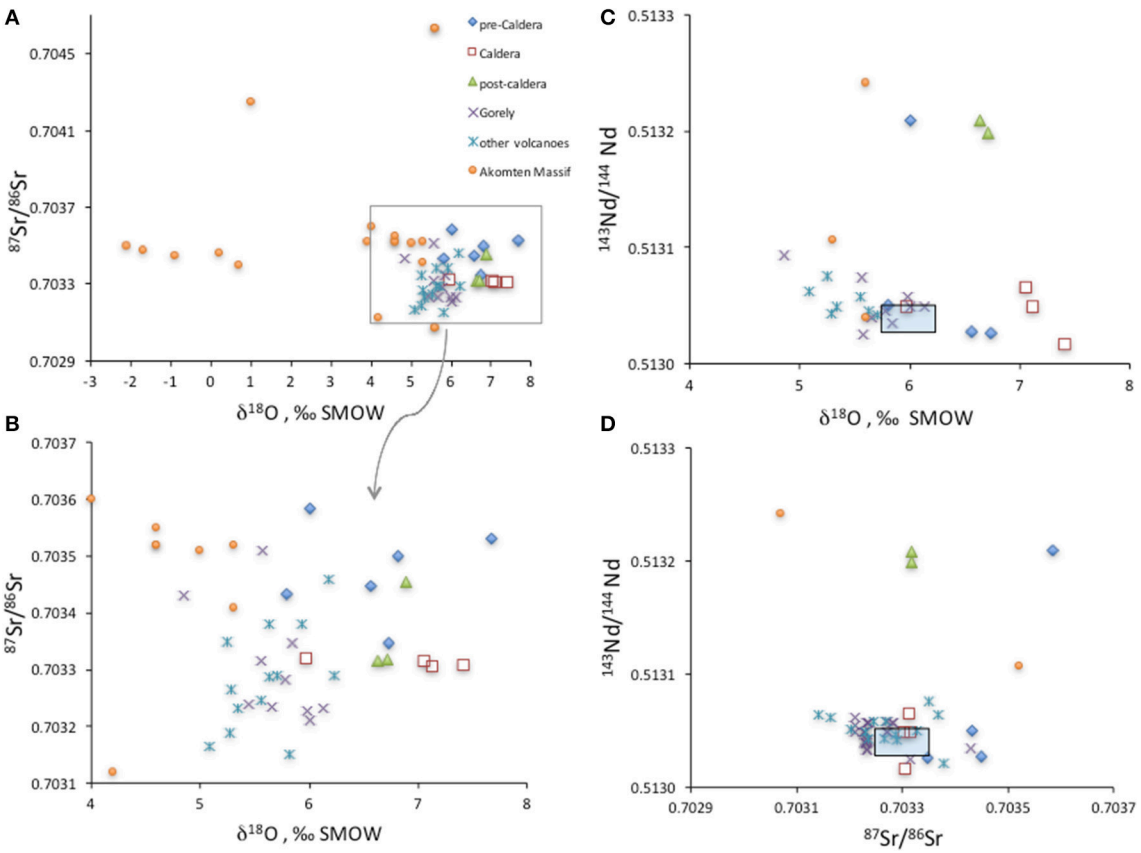

FIGURE 7 | Sr, Nd, and O isotopes in rocks from Karymshina Volcanic Complex in comparison to neighboring volcanoes, and basement rocks (Akhomten granite massif, and Ganal series metamorphics). Small rectangles in **(C,D)** indicate mantle derived basalts and products of their differentiation, and regional Sr and Nd isotopic values from central part of Eastern volcanic front Churikova et al. (2001) and Bindeman et al. (2004). **(A)** Regional pattern, showing low-$\delta^{18}O$ and diverse Sr isotopes in hydrothermally altered crust from Akhomten and overall normal to slightly high-$\delta^{18}O$ values of Karymshina magmas. **(B)** Zoom in on Karymshina and local volcanoes data showing low $\delta^{18}O$ magmas from multi-caldera Gorely volcano (Seligman et al., 2014) and decrease of Sr isotopes from pre to postcaldera stage. **(C)** Nd vs. O, and **(D)** Nd vs. Sr isotopes showing that isotopic ranges of magmas in and around Karymshina are best explained by isotopically diverse crust.

in the proportion of the mantle component with time, despite the increasing degree of differentiation (increase in SiO_2) of the erupted rhyolites (**Figure 5**); this observation serves as the basis for mass and thermal modeling below. Finally, isotopic heterogeneity of Sr and Nd decreases with youth, in line with oxygen isotopic and elemental results above.

Rhyolite-MELTS Modeling

We conducted an extensive set of crystallization and assimilation modeling experiments using the rhyolite-MELTS program of (Gualda et al., 2012; for further results of this modeling campaign, see Shipley, 2011). Several samples of basaltic magmas from nearby volcanoes were compared and we selected a basalt from the Gorely volcano (Seligman et al., 2014) as most closely resembling a primitive magma from which the Karymshina magmas may have been derived. For a crustal assimilant composition, we used an amphibolite partial melt taken from the experiments of Rapp and Watson (1995), which is referred to hereafter as APM. This generic composition was chosen because although there are no partial melting experiments that have been done on rocks found near the Karymshina Caldera, amphibolite is a common metamorphic rock in the Kamchatka Peninsula and in other continental arcs (Wyllie, 1984) is a plausible composition for the lower crust in Kamchatka (Baboshina et al., 2000; Geological Map of the Russian Federation, 2000). A silicified, hydrothermally altered rock, IC50, with SiO_2 contents of 81.34 wt% (referred to hereafter as HAR) was also used as an assimilant as this type of rock may also have been added to the magma, driving the observed minor depletion in $\delta^{18}O$.

Crystallization trials were run with 0 and 2.5 wt% H_2O in the initial basalt and with 0, 25, and 50 wt% APM and 0 and 10 wt% HAR. These trials were conducted at 2 kbar, 8 kbar, and a split starting at 8 kbar and moving to 2 kbar after 50 wt% crystallization. One set of trials using only the initial basalt compositions was conducted with equilibrium crystallization to verify that the compositions seen at the Karymshina caldera could not have been the result of equilibrium crystallization. All other trials were conducted assuming fractional crystallization. In the case of the split pressure trials, the change in pressure

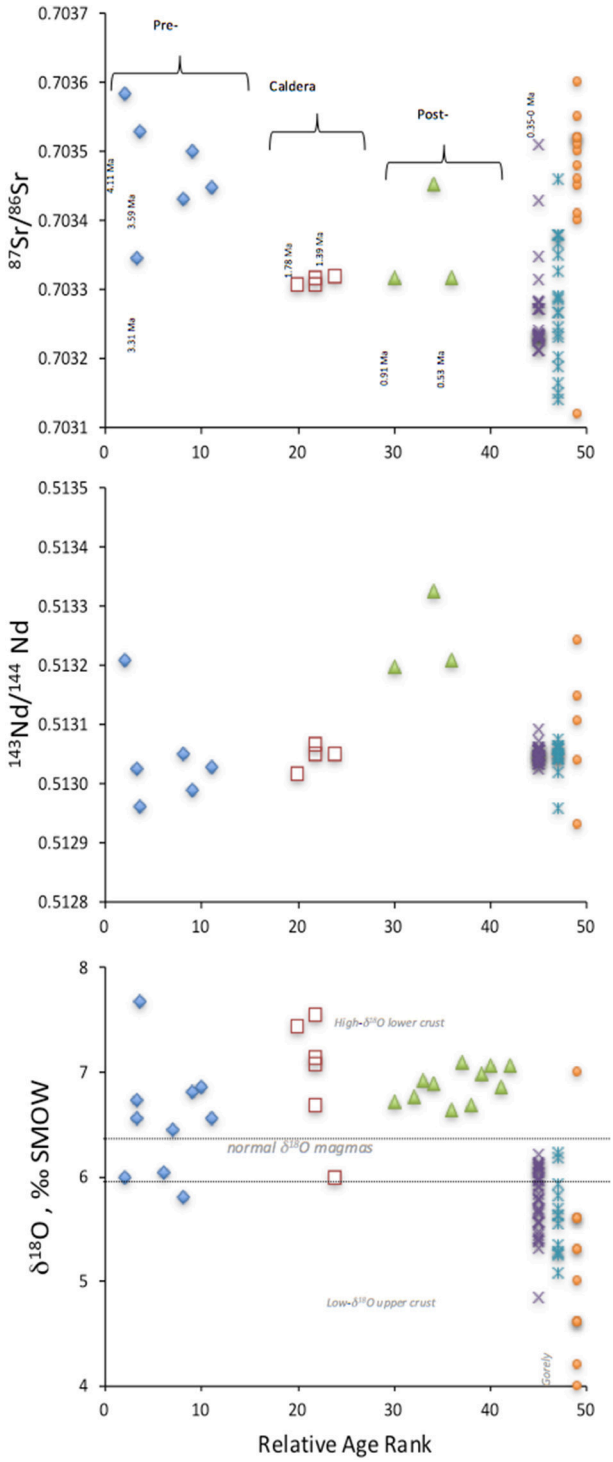

FIGURE 8 | Temporal evolution of the Karymshina Volcanic Complex in comparison to Gorely volcanic center (0–0.35 Ma, Seligman et al., 2014), other volcanoes nearby, and Akhomten granitic massif. Symbols are the same as on **Figure 7**. Units are plotted in relative random order except the ones indicated by arrows with ages from **Table 1** and **Figure 2** based on geochronology of this work and previously reported in Bindeman et al. (2010). Notice overall decrease in Sr and O isotopes, and increase in Nd isotopes from pre to postcaldera intrusions, and an increasing homogenization of isotopes with youth. Sr isotopes are adjusted to their initial values.

was assumed to be instantaneous based on the probable speed of magma ascent from Annen et al. (2006).

As expected, the results for equilibrium crystallization of the basaltic parent magma chosen show that it is impossible to obtain the rhyolitic composition of magma present at the Karymshina caldera. The results of the fractional crystallization trials obtained compositions closer to those observed at Karymshina; these results are shown in **Figure A3** for selected major elements. Most of the fractional crystallization trials resulted in strong enrichments of K_2O. This is most likely due to the initial basalt composition containing more K_2O than was present in the true parent magma of the Karymshina rocks. Fractional crystallization at shallow depths (2 kbar) resulted in the least enrichment of K_2O as well as a greater increase in the SiO_2 content of the remaining magma (**Figure A3**). The trials containing 50 wt% APM and 10 wt% HAR were closest to the actual K_2O and SiO_2 contents of the Karymshina rocks in all trials. Effects of addition of silica-rich HAR to plagioclase saturated magma are shown on **Figure 9**. In the 2 kbar trials, the magma with 2.5 wt% H_2O, 25 wt% APM, and 10 wt% HAR also matched well with the actual values measured in the Karymshina rocks. In the trials with 50 wt% APM, SiO_2 contents equal to those of Karymshina were obtained at all pressure options and approximately when 50 wt% of the magma was crystallized. The trials giving the best approximations of fractional crystallization leading to Karymshina magma compositions also match well with a straight line mixing trend between the initial basaltic magma and the rhyolites, indicating that the Karymshina magmatic series could also be the result of pure magma mixing between some higher-SiO_2 magma and a basaltic magma. If this is the case, the Karymshina magmas would likely be primarily composed of partial melts of amphibolite shallower hydrothermally altered rocks mixed with a small portion (<25 wt%) of basaltic magma.

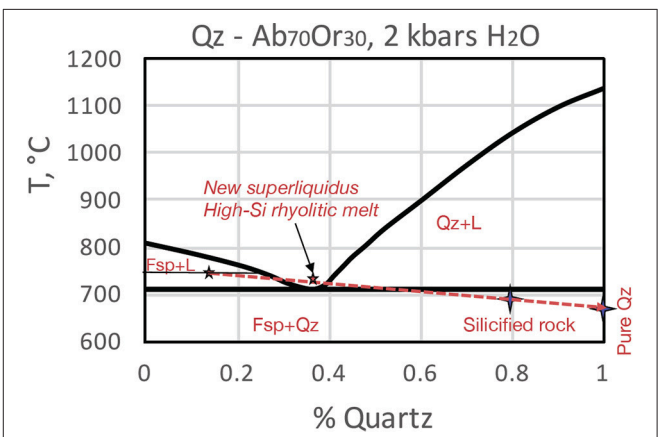

FIGURE 9 | A section through an experimental granite ternary (Tuttle and Bowen, 1958) at 2 kbars of water pressure and to the Ab side of Ab-Or cotectic. An explanation of addition of hydrothermally altered, silica-rich sinters and secondary quartz of diverse $\delta^{18}O$ values (large stars) into crystal-rich plagioclase-bearing rhyolites of Karymshina caldera (small star) to produce high-silica, crystal-poorer and lower temperature post-caldera extrusions. Addition of silicified rocks or silica-rich sinters causes composition-induced melting even if overall temperature of the system is dropping.

The results of the fractional crystallization trials for Al_2O_3, MgO, and CaO were similar to those for the K_2O and SiO_2 contents. The best fits for Al_2O_3 and MgO occurred with 0 and 2.5 wt% H_2O, 50 wt% APM, and 10 wt% HAR in the trial with pressures starting at 8 kbar and ending at 2 kbar. However, the trial at 2 kbar with 2.5 wt% H_2O, 50 wt% APM, and 10 wt% HAR is also a reasonable fit. In terms of CaO, the trials at 2 kbar and 2.5 wt% H_2O with 50 wt% APM and both 0 and 10 wt% HAR as well as the trial with 2.5 wt% H_2O, 25 wt% APM, and 10 wt% HAR are good fits to the Karymshina rocks. Thus, the fractional crystallization trial, which matched most closely the composition of the Karymshina rocks occurred at 2 kbar with 2.5 wt% H_2O, 50 wt% APM, and 10 wt% HAR. It should be noted that the rhyolite-MELTS runs approached but were not able to reproduce the most silicic compositions present at Karymshina. An additional amount of high-silica assimilant like the hydrothermally-altered rock may be required to produce these compositions, or the problem may lie with the formulation of various phase equilibria in the rhyolite-MELTS code.

Modeling using rhyolite-MELTS also requires that the $^{87}Sr/^{86}Sr$ and $^{144}Nd/^{143}Nd$ ratios of this APM be selected within the bounds provided by the Ganal metamorphic Massif (Vinogradov et al., 1991; Bindeman et al., 2004). These values are later diluted by the mantle-like cumulates or the plutonic equivalents of early stages of Karymshina volcanism. Based on the final isotopic values of the magmas, ∼10 wt% crustal material is added, the contribution of the crustal component would make up more than 50 wt% of the magma after more than 75% crystallization of the magma by fractional crystallization processes. This reconciliation of elemental and isotopic parameters predicts that the Sr and Nd values in the added crustal component and in the hydrothermally altered component may be closer to the mantle values, which is typical of Kamchatka.

Thermomechanical Modeling

The I2VIS program (Gerya and Yuen, 2003; Colón et al., 2018a,b) thermomechanical model was allowed to run for approximately 20 Myr of model time at a low mantle input rate averaging ∼200 km^2/Myr, producing significant intrusions of basalt and their cumulates in the crust. These intrusions are ∼60 km in width, similar in magnitude to the Kamchatkan arc, and thicken the crust from an initial value of 35 km (see animation in **Supplementary Material**) to nearly 50 km (**Figure 10**). This thickened crust is also significantly heated until the Moho temperature nears 1,000°C, making the lower crust both weak and dense as it metamorphoses to eclogite in the presence of minor partial melts (**Figure 10a**; the model uses the stability fields of Ito and Kennedy, 1971). Eventually, these conditions produce a Rayleigh-Taylor instability along the boundary between the crust and the mantle (**Figure 10b**). This instability produces a large drip of dense and relatively cool material, which detaches and sinks away from the crust in as little as 0.25 Myr (**Figure 10c**), followed by another instability and drip which forms about 1 Myr later (**Figure 10e**). These drips allow hot mantle to rise into shallower levels than before, producing huge temporary spikes in basaltic melting (**Figure 11a**), which in turn heats the overlying crust extremely rapidly and produces a surge of silicic melt production and volcanism (**Figures 11b,c**). In this delamination event, ∼1,500–2,000 km^3 of felsic rocks in total are erupted. This produces a caldera filled with silicic volcanic rocks (gray in **Figure 10e**), and thins the crust by several kilometers in the region (**Figure 10f**). Melt production quickly recovers to its pre-delamination rate (**Figure 11a**), again thickening the crust and producing another delamination event about 10 Myr after the first, which is accompanied by a similar surge in basalt production and accompanying felsic eruptions. Finally, we note that the delamination and rhyolite production events are characterized by drops in the ε_{Nd} values of the erupted felsic material, caused by spikes in crustal melting caused by the increased basalt intrusion rate.

A movie of delamination events is given as **Movie A1**.

DISCUSSION

High-Silica Rhyolites in Arc Settings and Mode of Their Genesis

True high silica rhyolites (HSR) that are represented by nearly all post-caldera Karymshina extrusions are generally rare in Kamchatka and other arc settings, where when they do occur are mostly found in arcs built on thick continental crust (e.g., Andes, de Silva and Gosnold, 2007; Folkes et al., 2011). HSRs are, by contrast, quite common in intracontinental extension or hotspot environments as can be seen via the GEOROC database. Small volume HSR magmas such as aplites (e.g., Waters and Lange, 2017) can be produced by extreme fractional crystallization of a bigger magma body or a series of such events, especially if they contain very few or no crystals. By contrast, the eruption of large volumes (100s of km^3) of ignimbrites or lavas of HSR magmas requires processing of an even greater volume of low silica rhyolitic crust, and in many cases HSR are associated with large volume (100s to 1,000s of km^3) rhyolitic or dacitic "monotonous intermediate," crystal-rich magmatic centers (Hildreth and Moorbath, 1988; Grocke et al., 2017). HSR extraction from batholithic-scale magma bodies of rhyolitic composition seems like a reasonable proposition (Bachmann and Bergantz, 2004; Watts et al., 2016), and thus HSR genesis requires crust-wide reworking (Lipman, 2007). Previous studies indicate that crust of at least 30 km in thickness is required to produce HSR magmas and the 40 km thickness found at Karymshina is most favorable (Hughes and Mahood, 2008; **Figure 2**). It should also be noted that thicker crust may provide more space for basaltic underplating of one or more differentiating magma bodies, allowing progressively more differentiated silicic partial melts to be sequestered upward through multiple melting-remelting episodes (e.g., Bindeman and Simakin, 2014). Large volumes of silicic magmatism would naturally require a greater proportion of basaltic magmas (Annen and Sparks, 2002; Annen et al., 2006) and we model the initial and final crustal thicknesses below.

Summary of Geologic and Geochronologic Trends in the Karymshina Volcanic Complex

New and compiled geochronology demonstrates the long-lived nature of the Karymshina Volcanic Complex, lasting from ∼4 to 0.5 Ma (**Figure 2**). Eruptions started at ∼4 Ma with quartz

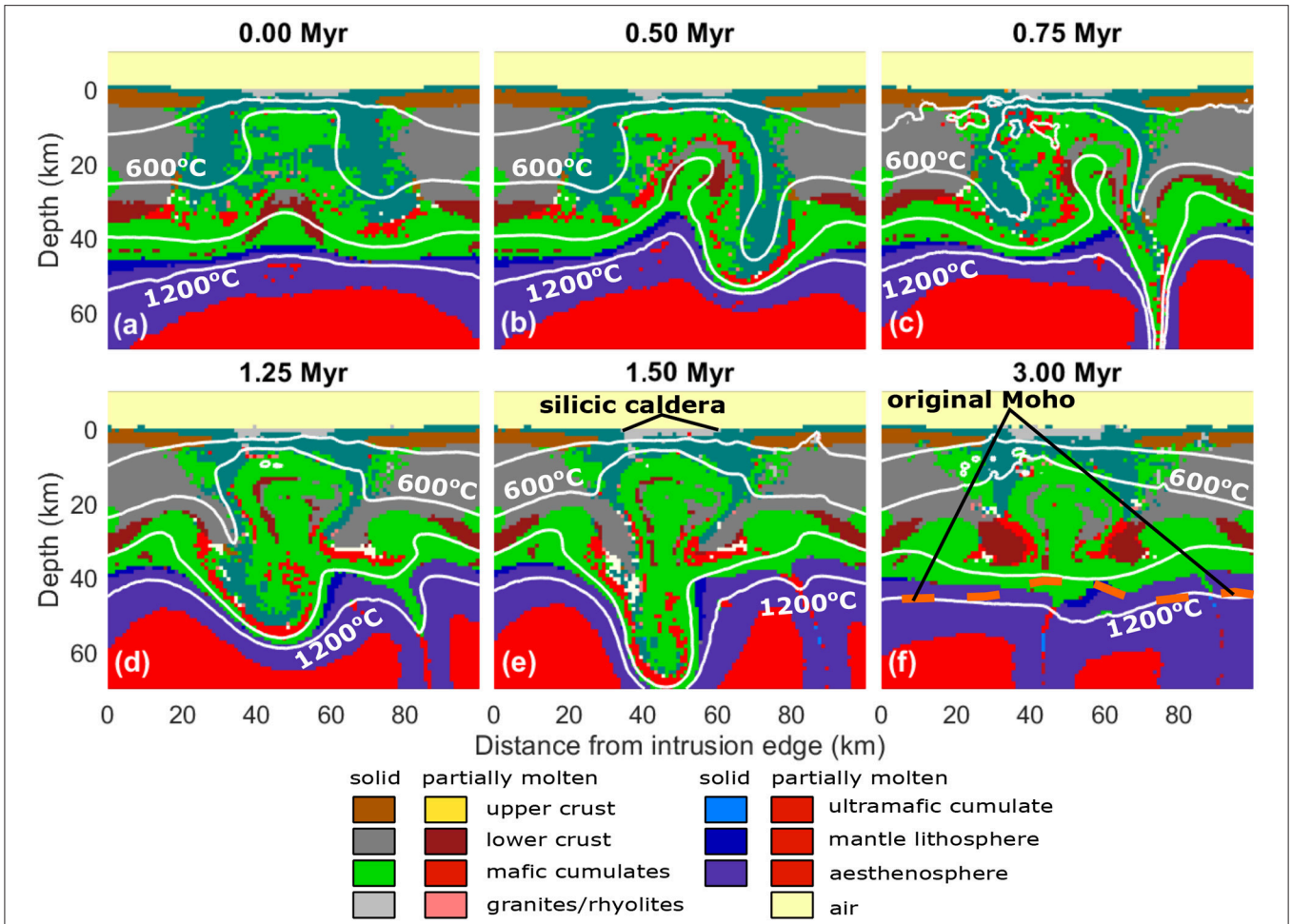

FIGURE 10 | Thermomechanical model of delamination-triggered mantle melting and surface volcanism. White lines are 200°C temperature contours. **(a)** 4 Myr after the initially 35 km-thick crust has been thickened to nearly 50 km by repeated additions of basalt to the crust, basalt addition and heating the crust results in the first signs of Rayleigh-Taylor instabilities in the Moho, **(b,c)** Over the next 1.25 Myr, this develops into a drip which removes the lowermost crust including most of the mafic cumulates, and continental lithosphere, drawing hot mantle up into the resulting space, and causing extensive melting. **(d,e)** From 1.5 to 2.5 Myr after the start of the delamination event, further delamination occurs on the left side of the model, causing another smaller surge of melting. **(f)** Finally, the lower crust cools and begins to solidify after the surge in mantle melting, and a new equilibrium with thinner, ∼30 km thick crust begins, starting a new cycle.

bearing biotite tuffs, and continued through 3.62 Ma. The older precaldera group eruptions of 3.4–3.6 Ma formed basaltic, basaltic andesitic and dacitic volcanoes. More geochronology is needed to establish the connection of these precaldera extrusions to the voluminous 1.78 Ma Karymshina ignimbrite, and to understand whether this initially diverse set of volcanic products represents the "waxing and pre-conditioning" the crust with basaltic melts that leads to crustal melting, as is described for the Andes by de Silva and Gosnold (2007) and for western North America by Lipman (2007). A caldera-forming episode at 1.78 Ma produced an estimated 800 km^3 of 71.5–73 wt% SiO_2 crystal-rich ignimbrite. After a rather significant time gap, HSR extrusions tracking the approximate caldera ring fractures erupted, with this last stage lasting from 0.9 to 0.5 Ma.

Thus, there appear to be three major eruptive periods, approximately 1 million years apart, a pre-caldera stage from 4 to 3.3 Ma, the caldera-forming eruption(s) at 1.78 Ma, and postcaldera eruptions from 0.9 to 0.5 Ma (**Figures 5**, **8**). As post-caldera extrusions are compositionally continuous (complementary) to the 1.78 Ma ignimbrites, they in theory could be extracted as residual melts from a caldera-wide crystalline mush (Bachmann and Bergantz, 2004) and diluted by hotter melts derived from the hot zone near the Moho with mantle-like Sr and Nd isotopes. However, the large time period between eruptions would indicate the presence of a crystalline mush from which the magma for both eruptions was supplied. This mush would have to be kept constantly heated up by basaltic intrusions to remain semi-molten state within the earth's crust for >1 Ma. The size of Karymshina eruptive center, the caldera dimensions, the duration of volcanism, the crystal-rich nature of eruptive products, and the presence of hydrous phases such as biotite and amphibole allows us to compare it to well-studied ignimbrite succession from the Cenozoic North American ignimbrite flareup (Lipman, 2007), and especially to the Andes (de Silva and Gosnold, 2007; Folkes et al., 2011). Ignimbrite flareups and continuous subsequent volcanism are conventionally interpreted

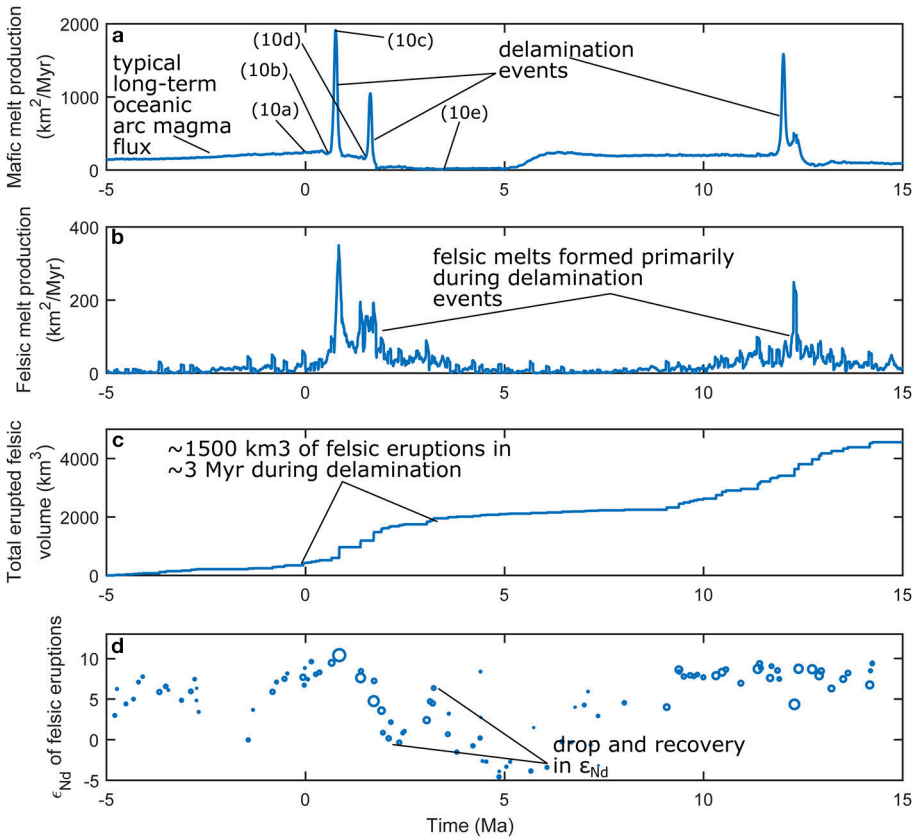

FIGURE 11 | Melt production and volcanism during the delamination event depicted in **Figure 10**. **(a)** The surge in mantle melting lasts <2 Myr, and is punctuated by sharp spikes associated with the actual dripping events. **(b)** The increase in mantle melting is associated with a coeval spike in the production of felsic melts in the crust (including intrusions), and **(c)** in the rate of eruption of rhyolites on the surface (to calculate 3D volumes here we assume a model thickness of 20 km). **(d)** Finally, we note that the surge in rhyolitic volcanism is associated with a noticeable drop in ε_{Hf} used in our models (which linearly correlates with ε_{Nd}) values as a result of a surge of crustal melting. This demonstrates that an increase in mantle melting alone can trigger a drop in ε_{Nd} values, making the underthrusting of fertile crustal material not necessary for all such arc flareup events (Ducea and Barton, 2007; DeCelles et al., 2009).

as resulting from periodic rejuvenation of a batholithic scale mushy magma chamber of rhyolitic composition, from which interstitial high-silica rhyolitic liquids are periodically extracted. The most likely reason for rejuvenation of a nearly frozen yet wet magma system is the continuous supply of basaltic magma, resulting in a variety of segregation processes described in the literature (e.g., Bachmann and Bergantz, 2006; Huber et al., 2011). Given the size of the magma chamber necessary to produce such large volumes of volcanic HSR, comparatively small amounts of basaltic magma likely intruded into the crystalline mush without much mixing with it, avoiding a significant impact on the overall constant composition of the postcaldera intrusions. Based on the hot spring activity near the Karymshina caldera, the last dated eruption at 0.5 Ma, and the overall long cooling timescales of batholith-scale magma bodies (Glazner et al., 2004; Lipman, 2007), it is quite probable that Karymshina is not a fully finished magmatic system despite its uplift and erosion, and that another episode of intracaldera basalt intrusion and rejuvenation would trigger another extrusive dome eruption.

Pacific Sediment Cores and 1.78 Ma Karymshina Eruption

No thick ∼1.78 Ma ash layers in the ODDP 882 and 883 Pacific cores (Cao et al., 1995) compositionally matched the Karymshina ignimbrite despite comparable mineralogy (**Figure 12**). It should be noted that we only analyzed thick 6 to 10 cm ash layers that were within a 0.06–0.12 Ma vicinity of the 1.78 Ma Karymshina age, and did not sample <1 cm ash layers that may also correspond to the 1.78 Ma eruption. We conclude that either the 1.78 Ma Karymshina eruption did not generate a large enough ash cloud to spread to the southwest of the Pacific, which seems surprising given the large estimated size of the caldera and several hundred km^3 inferred volume of the associated eruption (**Figure 2**; Bindeman et al., 2010), or that the winds during the eruption may instead have distributed ash in a different direction. Future efforts should examine cores from the Sea of Okhotsk.

We also compare ash from appropriate stratigraphic intervals to the 0.44 Ma Pauzhetka and 0.3 Ma Gorely caldera eruptions studied simultaneously in the same cores. Three ash layers are partially matched to the Pauzhetka composition, especially in

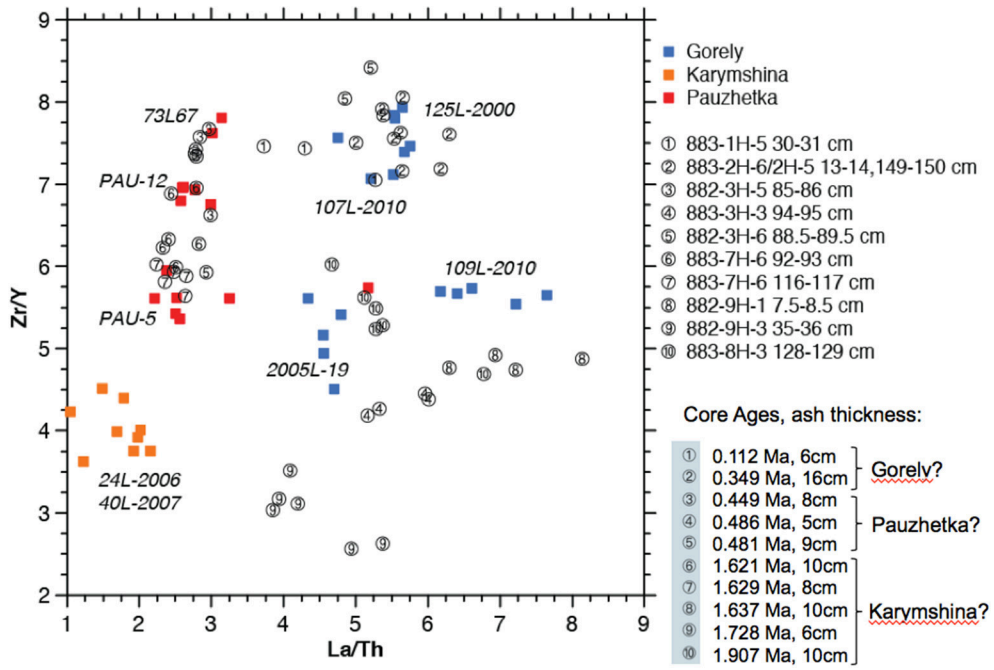

FIGURE 12 | Trace elemental ratio diagram comparing interstitial glass in the 1.78Ma Karymshina ignimbrite and other studied Kamchatkan tephras as compared to the Pacific cores ODDP-882 and 883. Note the match of Pauzhetka and Gorely tephra layers but lack of match for Karymshina. Age and ash thickness data is from Prueher and Rea (2001). See text for discussion and **Table A2** for analyses of analyzed tephras.

Zr/Y and La/Th: 882-3H-5 at 85–86 cm, 883-7H-6 at 92–93 cm, and 883-7H-6 at 116–117 cm. Ponomareva et al. (2018) recently identified Pauzhetka ash in cores from the Pacific and the Sea of Okhotsk via trace elemental match of and calibrated its astrochronologic age to 0.426 Ma.

Isotopic and Trace Elemental Trends

Sr, Nd, and O isotopic trends seen in **Figures 7**, **8** indicate the following.

(1) Erupted magmas have overall mantle-like compositions, suggesting that mafic magma differentiation and the melting of similar young Cenozoic crust can explain the abundant silicic rocks of Karymshina Eruptive Center. (2) Decreasing diversity of these isotopes through time is consistent with the formation of a homogenous batholith-scale magma body prior to the 1.78 Ma eruption. (3) Decreasing $^{87}Sr/^{86}Sr$ and increasing $^{143}Nd/^{144}Nd$ isotopic ratios with youth suggest that the system received continuous inputs from mantle-derived basalt or products of its differentiation (**Figure 8**), thus mantle-derived basalt and products of its differentiation not only contributed heat but participated materially in the petrogenesis of silicic magmas. (4) The youngest group of postcaldera rhyolites, which are true high-silica rhyolites, have the greatest proportion of this mantle component, which seems counter intuitive, given that these magmas are most differentiated. (5) Compatible trace elemental concentrations and their ratios to incompatible elements decrease in diversity and values through time, also consistent with the proposed homogenization of magma reservoir followed by sequestration to more differentiated values. (5) Zr saturation temperatures also decrease with youth. (6) Oxygen isotopes indicate decreasing diversity and requires contributions from high-$\delta^{18}O$ mantle sources and low-$\delta^{18}O$ hydrothermally altered crust. These results are confirmed by zircon $\delta^{18}O$ diversity in the caldera-forming ignimbrite (Bindeman and Simakin, 2014). Finally, (7), potentially supporting evidence for the role of hydrothermal alteration comes from low D/H ratios in amphiboles and biotites (**Figure 6**). However, the final Karymshina magmas are not low-$\delta^{18}O$ in absolute sense, i.e., lower than the mantle-derived differentiate (<6–6.3‰).

Model for Karymshina Silicic Volcanism

The formation of voluminous magmas with rhyolitic (70–74 wt% SiO_2) and especially high-silica rhyolitic (>74 wt% SiO_2) compositions is currently a topic of hot debate in the geologic community (Bachmann and Bergantz, 2004, 2008; Annen et al., 2006; Lipman, 2007; Watts et al., 2011, 2016; Bindeman and Simakin, 2014; Colón et al., 2015). Four end-member processes by which these magmas can form are (1) the fractional crystallization of a basaltic parent, (2) extraction of evolved melt from an evolved crystalline mush, (3) underplating and melting of pre-existing crust or previous cumulates in a "hot zone," and (4) shallow recycling and remelting of erupted and subvolcanic products of already differentiated, commonly hydrothermally altered, composition.

These are not all mutually exclusive and it is likely that the Karymshina magmas were formed by a combination of these mechanisms. The deep crustal hot zone method allows for partial melting of the crust, which would incorporate a crustal

component especially as the magma would be buoyant and rise through the crust where it would stall out in a shallow magma chamber (Annen et al., 2006). This deep crustal hot zone would also provide a constant source of magma recharge and heat to the developing magma chamber located at shallower depths. The partial melting of Eocene and younger Kamchatkan crust would also produce a component with high SiO_2 (Rapp and Watson, 1995) and in larger volume, which is necessary according to our MELTS modeling to achieve voluminous rhyolitic compositions. The siliceous crustal partial melt is needed because fractional crystallization alone will not sufficiently raise the SiO_2 content to the levels observed in Karymshina (and similar examples wordwide) rocks, and in sufficient volumes. However, there must also be large amounts (ca 50%) of fractional crystallization to obtain the highest SiO_2 levels observed, which could occur by internal differentiation within a long-lived magma chamber with a crystalline mush (Lipman, 2007; Bachmann and Bergantz, 2008). Finally, in the shallow crust where the crystalline mush (representing the shallow portion of the crystallizing upper crustal batholith) would most likely reside, incorporation of recycled and remelted material would occur, including a small amount of locally silicified, hydrothermally altered crust with very high SiO_2 contents and low $\delta^{18}O$ and δD values (**Figure 6**). This hydrothermally-altered crust must have been incorporated into the magma to allow for the final increase in SiO_2 content to bring the magma to the composition observed. Such a model would also account for the range of values around normal mantle-like $\delta^{18}O$ values in the population of zircon phenocrysts.

Here we propose an additional simple mechanism of obtaining high-silica rhyolite by assimilation and melting of silica-rich hydrothermally altered rocks. Evidence of hydrothermal activity in and around the Karymshina caldera, the presence of inclusions of hydrothermal sinters in the products of Karymshina eruptions, and rhyolite-MELTS experiments that would favor addition of silica-rich compositions to obtain the postcaldera high silica rhyolites makes us to propose a simple model for generating moderate volumes of HSRs using rocks silicified by hydrothermal activity over a period of several million years since initiation of silicic magmatism at 4 Ma. **Figure 9** explains this concept and permits an increase in melt fraction even if there is an addition of nearly isothermal higher silica assimilant. Postcaldera high-silica rhyolitic intrusions have lower Zr saturation temperatures than the 1.78 Ma ignimbrite but contain fewer crystals. Simakin and Bindeman (2012) modeled the situation of excess silica in roof rocks above a magma body and observed no mechanical benefit of eroding low silica vs. a silica oversaturated roof. However, addition of such a high-silica rock permits an increase in melt fractions, which aids in obtaining high silica compositions.

In many recent models of crustal melting and granitic magma differentiation (Annen et al., 2006; Bohrson et al., 2014; Colón et al., 2018b, and many others), the amount of basalt that is required to generate silicic differentiates and provide heat for batholith-scale crustal melting equates to the added thickness of 10–15 km. As crustal thickening producing a cumulate-restite root of this magnitude is not observed in Karymshina seismic images (**Figure 3**) or other similar examples of large volume silicic centers around the world, effective delamination of the lower crust back into the mantle on timescales comparable to the duration of magmatic flare-ups (a few Myr), is required.

Thermomechanical Modeling

Like Yellowstone (Colón et al., 2018a,b), Karymshina is uniquely suited to the type of large-scale thermomechanical modeling we employ here, not only because of the numerous constraints placed on it by this and previous studies, but also because its large size and significant duration make it computationally approachable for models that have relatively long timesteps (5 kyr, in this case), and large regional-scale computation grids with resolutions of 1–2 km, as we use here. We here discuss preliminary results of attempts to model voluminous silicic systems in a subduction setting using the I2VIS code.

We begin with a relatively weak mantle plume as a melt source in the model, with a basalt production rate of approximately 200 km^3/km/Myr of arc (**Figure 11a**), which is in line with the long-term island arc melt production rates calculated by Jicha and Jagoutz (2015). This mantle melting heats and thickens the crust for nearly 20 Myr prior to the time interval which we examine in **Figures 10**, **11**, which marks the appearance of the first Rayleigh-Taylor instabilities at the Moho (**Figure 10a**). At this point, we see two crustal dripping events separated by about 1 Myr occur, the second triggered by the first, which produces a surge of mantle melting leading to the eruption of ∼1,500 km^3 of felsic magmas on the surface. These events occur spontaneously after heating and thickening of the crust by the steady intrusion of basalt renders the system unstable. By 3 Myr after the appearance of the initial instability, the system has returned to relative equilibrium (**Figure 10f**), with notably less dense cumulate material (green in **Figure 10**) in the lower crust, and resumes thickening until another delamination event occurs 10 Myrs later. We further note that the thickness of the crust decreases from an intital amount of ∼45 km (outlined by the orange dashed line in **Figure 10e** and the original geometry of **Figure 11a**) to a lesser value of about 40 km. The fallen cold material initially disrupts the hot plume in the mantle, producing a lull in basalt production (**Figure 11a**), but the system quickly recovers to a steady-state of mantle melting after a few Myr. Future modeling efforts with a more realistic subduction geometry will help to determine whether such a lull could also be expected to occur in an actual subduction zone rather than the mantle plume-driven model we use here.

The duration of this delamination event in our model is tantalizingly similar to the duration of volcanism at Karymshina, suggesting that such an event may explain the large but apparently temporary felsic melting flare up observed there since 4 Ma. The current crustal thickness at Karymshina of 38 km (**Figure 3**) is up to 5 km less than the surrounding area, suggesting that material below the caldera may have been lost to the mantle. The scale of the silicic volcanics-filled caldera which develops in **Figures 10e,f** (gray material), which is about 20 km wide and 3 km deep, also is quite similar to that seen at Karymshina (**Figures 2**, **3**). Finally, we use Nd isotopes as a

proxy in the model for the amount of crustal melting occurring, assuming that they can be compared to any other radiogenic isotope system such as Sr or Hf. For **Figure 11d**, we assume that the entire crust has a $^{143}Nd/^{144}Nd$ value of 0.51237 ($\varepsilon_{Nd} = -5$) and that the mantle and its melts have a highly depleted $^{143}Nd/^{144}Nd$ value of 0.5133 ($\varepsilon_{Nd} = +13$). While our model does not directly replicate the values seen in **Figure 7**, we identify a few clear trends. First, we see that the first delamination event (the one shown in **Figure 10**) is associated with a clear excursion toward more unradiogenic (crust-like) values in the initial eruptions, followed by a rapid recovery to more mantle-like values. This trend is less clear in the second delamination event seen in **Figure 11**, but this may be because the crustal material in the model has been more consumed by then and the crust and is no longer available to melt. As for the times between delamination events, such as at 5 Myr, we currently suspect that the model overestimates the crustal melt contribution to erupted rhyolites at very low fluxes, particularly from the lower crust, as these low-percentage melts may be too efficiently extracted, skewing the behavior of the isotopes in **Figure 11d** outside of delamination events. In general, the tendency to recover back to mantle-like values after excursions of crustal melting reflects the "basaltification" of the crust during high-flux volcanic periods discussed above. The initial drop in ε_{Nd} suggests that the crust-like radiogenic isotope signature commonly seen in arc flare-ups (DeCelles et al., 2009) may simply be a result of hotter systems being associated with more rapid rates of intrusion being able to produce more crustal melting. Cooler systems, such as those associated with the post-caldera HSR eruptions at Karymshina, are able to fractionate mantle-derived basalts and the intrusions they produce, but with little excess heat available to melt the crust.

While these modeling results are highly preliminary, they offer a tantalizing glimpse into the potential origins of short-lived large caldera systems like Karymshina in arcs otherwise dominated by more typical stratovolcanoes and shields. Further modeling efforts will need to use more realistic geometries for the crust and mantle, including a fully-realized subducting slab-mantle wedge system, and hopefully 3D modeling to fully capture the inherently non-planar phenomena of delamination and dripping of the lithosphere. Further investigating this problem, and coupling it more closely to the precise geology and geochemistry of arc caldera systems like Karymshina promises to be an exciting field of future research.

CONCLUSIONS

Our observation and modeling suggests that the generation of voluminous rhyolitic and high-silica rhyolitic magmas at the Karymshina Caldera is most likely due to a combination of magma intrusion into a deep crustal hot zone that has led to incremental shallow batholith formation in the upper crust with shallow phenocryst assemblages. This is achieved by incubation by repeated intrusions followed by fractional crystallization in a large magma body. In addition, at shallow depths, a small amount of hydrothermally-altered crustal rock with extremely high SiO_2 content must also have been incorporated into the magma.

Three rhyolitic eruptive periods, at ∼4 Ma, prior to caldera-formation at 1.78 Ma, and the one encompassing the post-caldera extrusions between 0.9 and 0.5 Ma indicate the incremental assembly of a long-lived silicic upper crustal batholith magma body kept in various thermal states throughout its history. The proportion of mantle derived Sr and Nd and crustal derived H is increasing with time advocating progressive "basaltification" of the system in which siliceous differentiates of basaltic magmas dilute the signatures of the original crustal remelts of the initial stages of magmatism.

Geochemically, the 0.9–0.5 Ma post-caldera extrusions appear to be directly evolved from fractional crystallization of the caldera-forming magma; thus in response to continuing basaltic input, this upper crustal rhyolitic body is undergoing internal fractional crystallization to generate homogenous, crystal poorer, high-silica post-caldera rhyolites.

At the typical 0.001 km^3/yr eruption rate, the hydrous basalt intruded into a 38 km typical Kamchatkan arc crust produces two magma bodies, one near the Moho and the other engulfing the entire section of upper crust. Basalt is trapped in the lower portion of the upper crustal magma body, which exists as partially molten to solid state. Differentiation products of basalt periodically mix with the resident magma diluting its crustal isotopic signatures. At the end of the magmatism crust is thickened by 8 km.

Thermomechanical modeling suggests that following a long incubation period of basaltic intrusions, delamination of the lowermost crust and mantle lithosphere due to overthickening can produce brief but extremely intense magmatic flareups which may drive the higher intrusion rates that replace typical arc volcanic behavior with voluminous, caldera-forming eruptions.

Magmatic episodes lasting several million years under the continental arc of Kamchatka in systems comparable to Karymshina lead to crust-wide material redistribution and sequestration of silicic products to the upper crust, likely leading to local batholith formation.

Future Directions

Given the abundant presence of hot springs in the area around the Karymshina magma body, it is important to determine by geophysical methods if magma is still present and is crystallizing beneath the caldera. The compositions of the caldera-forming ignimbrites and the post-caldera extrusions show a high degree of homogeneity, which would also be consistent with extraction of a melt from a large-scale crystallizing mush. Ar-Ar dating of post caldera intrusions should aim at finding the youngest magmatic rock which currently stands at 0.5 Ma. Future research should also concentrate on the search for extracaldera ignimbrites coeval to the 1 km thick 1.78 Ma intracaldera tuff. A lack of topographical expression of the caldera walls presents a problem, but may be due to a combination of erosion by glaciers during the last glacial maximum, tectonic movement along faults, and high rates of erosion during modern times. Further mapping and recognition of collapse features (lag breccia, mega blocks, etc.) is required. Recognition of the 1.78 Ma and older deposits in the sediment cores in the Pacific and the Sea of Okhotsk is required. Finally, our very preliminary thermomechanical models suggest

an important role for lithospheric dripping and delamination for driving arc caldera volcanism, which promises to be a fruitful area of future inquiry.

AUTHOR CONTRIBUTIONS

IB conceived the study and executed most of the effort. DC used TG computer program to perform thermomechanical modeling. VL (deceased 2016) and AR contributed fieldwork, samples, and map for the study. NS defended MS thesis under IB on geochemistry of rocks. BJ did Ar-Ar dating. ML determined the chemistry of Pacific ashes and ignimbrite. All authors read the paper and discussed results.

FUNDING

USA NSF grants # EAR 0537872 and EAR 1822977 to IB, and RNF Russian Science Foundation grant #16-17-10035 to VL and AR. Part of work is a based on cited and published thesis by a coauthor NS.

ACKNOWLEDGMENTS

We thank Michel Grègoire (OMP Toulouse), a reviewer and Pavel Izbekov, as well as Katie Dobson for editorial handling. Any use of trade, firm, or product names is for descriptive purposes only and does not imply endorsement by the U.S. Government.

SUPPLEMENTARY MATERIAL

The Supplementary Material for this article can be found online at: https://www.frontiersin.org/articles/10.3389/feart.2018.00238/full#supplementary-material

Table A1 | Chemical analyses of Karymshina Volcanic Center samples used in this study.

Table A2 | Results from North Pacific tephra and Kamchatka volcano glass.

Table A3 | Electron microprobe analyses of mineral phases and glass in ignimbrite and post-caldera extrusions. Done at University of Oregon (John Donovan, analyst).

Table A4 | Details of Ar-Ar dating of studied samples.

Figure A1 | Elemental temporal trends through Karymshina.

Figure A2 | Plag-Qz plots for Karymshina rocks.

Figure A3 | Results of rhyolite MELTS fractional crystallization at 8 and 2 kbars. Pressure with 2.5 wt% of H_2O in the initial. Best match is provided by 75% crystallization at low pressure with addition of 25% of amphibolite partial melt and addition of 10% silica-rich, hydrothermally-altered rocks.

Movie A1 | Delamination events in the course of our modeling.

REFERENCES

Anderson, A. T., Davis, A. M., and Lu, F. (2000). Evolution of Bishop Tuff rhyolitic magma based on melt and magnetite inclusions and zoned phenocrysts. *J. Petrol.* 41, 440–473. doi: 10.1093/petrology/41.3.449

Annen, C., Blundy, J. D., and Sparks, R. S. J. (2006). The Genesis of intermediate and Silicic magmas in deep crustal hot zones. *J. Petrol.* 47, 505–539. doi: 10.1093/petrology/egi084

Annen, C., and Sparks, R. S. J. (2002). Effects of repetitive emplacement of basaltic intrusionson thermal evolution and melt generation in the crust. *Earth Planet. Sci. Lett.* 203, 937–955. doi: 10.1016/S0012-821X(02)00929-9

Baboshina, V. A., Tereshchenkov, A. A., and Kharakhinov, V. V. (2000). *Tectonic Map ofthe Sea of Okhotsk Region*. Institute of the Lithosphere of Marginal Seas, Russian Academy of Sciences, Scale 1:6,500,000, 1 sheet.

Bachmann, O., and Bergantz, G. W. (2004). On the origin of crystal-poor rhyolites: extracted from batholithic crystal mushes. *J. Petrol.* 45, 1565–1582. doi: 10.1093/petrology/egh019

Bachmann, O., and Bergantz, G. W. (2006). Gas percolation in upper-crustal silicic crystal mushes as a mechanism for upward heat advection and rejuvenation of near-solidus magma bodies. *J. Volcanol. Geotherm. Res.* 149 , 85–102 doi: 10.1016/j.jvolgeores.2005.06.002

Bachmann, O., and Bergantz, G. W. (2008). Rhyolites and their source mushes across tectonic settings. *J. Petrol.* 49, 2277–2285. doi: 10.1093/petrology/egn068

Bacon, C. R. (1983). Eruptive history of mount Mazama and Crater Lake caldera Cascade Range USA. *J. Volcanol. Geotherm. Res.* 18, 57–115. doi: 10.1016/0377-0273(83)90004-5

Bindeman, I. N., Anikin, A. P., and Schmitt, A. K. (2016). Archean xenocrysts in modern volcanic rocks from Kamchatka - insight into the basement and paleodrainage. *J. Geol.* 124:684833. doi: 10.1086/684833

Bindeman, I. N., and Bailey, J. C. (1994). A model of reverse differentiation at Dikii Greben' Volcano, Kamchatka: progressive basic magma vesiculation in a silicic magma chamber. *Contrib. Mineral. Petrol.* 117, 263–278.

Bindeman, I. N., Leonov, V. L., Izbekov, P. E., Ponomareva, V. V., Watts, K. E., Shipley, N. K., et al. (2010). Large-volume silicic volcanism in Kamchatka: Ar-Ar and U-Pb ages, isotopic, and geochemical characteristics of major pre-Holocene caldera-forming eruptions. *J. Volcanol. Geotherm. Res.* 189, 57–80. doi: 10.1016/j.jvolgeores.2009.10.009

Bindeman, I. N., Ponomareva, V. V., Bailey, J. C., and Valley, J. W. (2004). Volcanic arc of Kamchatka: a province with high-δ18O magma sources and large-scale 18O/16O depletion of the upper crust. *Geochim. Cosmochim. Acta* 68, 841–865. doi: 10.1016/j.gca.2003.07.009

Bindeman, I. N., and Simakin, A. G. (2014). Rhyolites – hard to produce but easy to recycle and sequester: integrating microgeochemical observations and numerical models. *Geosphere* 10, 930–957. doi: 10.1130/GES00969.1

Bindeman, I. N., Vinogradov, V. I., Valley, J. W., Wooden, J. L., and Natalin, B. A. (2002).Archean protolith, and accretion of crust in Kamchatka: SHRIMP dating of zircons from metamorphic rocks of Sredinny and Ganal Massifs. *J. Geol.* 110, 271–289. doi: 10.1086/339532

Bohrson, W. A., Spera, F. J., Ghiorso, M. S., Brown, G. A., Creamer, J. B., and Mayfield, A. (2014). Thermodynamic model for energy-constrained open-system evolution of crustal magma bodies undergoing simultaneous recharge, assimilation and crystallization: the magma chamber simulator. *J. Petrol.* 55, 1685–1717. doi: 10.1093/petrology/egu036

Budd, D., Troll, V., Deegan, F. M., Jolis, E. M., Smith, V. C., Whitehouse, M. J., et al. (2017). Magma reservoir dynamics at Toba caldera, Indonesia, recorded by oxygen isotope zoning in quartz. *Nature Sci. Rep.* 7:40624. doi: 10.1038/srep40624

Cao, L. Q., Arculus, R. J., and McKelvey, B. C. (1995). "Geochemistry and petrology of volcanic ashes recovered from Sites 881 through 884: a temporal record of Kamchatka and Kurile volcanism," in *Proceedings of the Ocean Drilling Program, Scientiic Results,* vol. 145, eds D. K. Rea, I. A. Basov, D. W. Scholl, and J. F. Allan (College Station, TX: Ocean Drilling Program), 345–381.

Chesner, C. A. (1998). Petrogenesis of the Toba Tuffs, Sumatra, Indonesia. *J. Petrol.* 39, 397–438. doi: 10.1093/petroj/39.3.397

Churikova, T., Dorendorf, F., and Woerner, G. (2001). Sources and fluids in the mantle wedge below Kamchatka, evidence from across-arc geochemical variation. *J. Petrol.* 42, 1567–1593. doi: 10.1093/petrology/42.8.1567

Colón, D. P., Bindeman, I. N., Ellis, B. S., Schmitt, A. K., and Fisher, C. M. (2015). Hydrothermal alteration and batch melting of crust by Columbia River Basalt magmas, fingerprinted by post-CRB rhyolites of the J-P Desert and the Jarbidge Mountains, Idaho and Nevada, USA. *Lithos* 224, 310–323. doi: 10.1016/j.lithos.2015.02.022

Colón, D. P., Bindeman, I. N., and Gerya, T. V. (2018a). Thermomechanical modeling of the formation of a multilevel, crustal-scale magmatic system by the Yellowstone Plume. *Geophys. Res. Lett.* 45, 3873–3879. doi: 10.1029/2018GL077090

Colón, D. P., Bindeman, I. N., and Gerya, T. V. (2018b). Understanding the isotopic and chemical evolution of Yellowstone hot spot magmatism using magmatic-thermomechanical modeling. *J. Volcanol. Geotherm. Res.* doi: 10.1016/j.jvolgeores.2018.12.003. [Epub ahead of print].

Colón, D. P., Bindeman, I. N., Wotzlaw, J.-F., Christiansen, E. H., and Stern, R. A. (2018c). Origins and evolution of rhyolitic magmas in the central Snake River Plain: insights from coupled high-precision geochronology, oxygen isotope, and hafnium isotope analyses of zircon. *Contrib. Mineral. Petrol.* 173:11. doi: 10.1007/s00410-017-1437-y

de Silva, S. (2008). Arc magmatism, calderas, and supervolcanoes. *Geology* 36, 671–672. doi: 10.1130/focus082008.1

de Silva, S. L., and Gosnold, W. D. (2007). Episodic construction of batholiths: Insights from the spatiotemporal development of an ignimbrite flare-up. *J. Volcanol. Geotherm. Res.* 167, 320–335. doi: 10.1016/j.jvolgeores.2007.07.015

de Silva, S. L., Zandt, G., Trumbull, G., Viramonte, J. G., Salas, G., and Jimenez, N. (2006). "Large ignimbrite eruptions and volcano-tectonic depressions in the Cen- tral Andes: a thermomechanical perspective," in *Mechanisms of Activity and Unrest at Large Calderas,* eds C. Troise, et al., (London: Geological Society of London Special Publication), 47–63

DeCelles, P. G., Ducea, M. N., Kapp, P., and Zandt, G. (2009). Cyclicity in Cordilleran orogenic systems. *Nat. Geosci.* 2:251. doi: 10.1038/ngeo469

Ducea, M. N., and Barton, M. D. (2007). Igniting flare-up events in Cordilleran arcs. *Geology* 3, 1047–1050. doi: 10.1130/G23898A.1

Ducea, M. N., Paterson, S. R., and DeCelles, P. G. (2015a). High-volume magmatic events in subduction systems. *Elements* 11, 99–104. doi: 10.2113/gselements.11.2.99

Ducea, M. N., Saleeby, J. B., and Bergantz, G. (2015b). The architecture, chemistry, and evolution of continental magmatic arcs. *Annu. Rev. Earth Planet. Sci.* 43, 299–331. doi: 10.1146/annurev-earth-060614-105049

Dufek, J., and Bergantz, G. W. (2005). Lower crustal magma genesis and preservation: a stochastic framework for the evaluation of basalt–crust interaction. *J. Petrol.* 46, 2167–2195. doi: 10.1093/petrology/egi049

Duggen, S., Portnyagin, M., Baker, J., Ulfbeck, D., Hoernle, K., Garbe-Schönberg, D., et al. (2007). Drastic shift in lava geochemistry in the volcanic-front to rear-arc region of the Southern Kamchatkan subduction zone: evidence for the transition from slab surface dehydration to sediment melting. *Geochim. Cosmochim. Acta* 71, 452–480. doi: 10.1016/j.gca.2006.09.018

Eichelberger, J. C., Izbekov, P. E., and Browne, B. L. (2006). Bulk chemical trends at arc volcanoes are not liquid lines of descent. *Lithos* 87, 135–154. doi: 10.1016/j.lithos.2005.05.006

Folkes, C., de Silva, S., Schmitt, A., and Cas, R. (2011). A reconnaissance of U-Pb zircon ages in the Cerro Galán system, NW Argentina: prolonged magma residence, crystal recycling and crustal assimilation. *J. Volcanol. Geothermal Res.* 206, 136–147. doi: 10.1016/j.jvolgeores.2011.06.001

Geological Map of the Russian Federation (2000). Panel N-57-XXVII (Petropavlovsk-Kamchatky) and Explanatory Notes, scale 1:200000, St Petersburg, VSEGEI Publisher, T.V. Brezhneva and LS Chelnokova (eds), (in Russian)

Gerya, T. V., and Yuen, D. A. (2003). Characteristics-based marker-in-cell method with conservative finite-differences schemes for modeling geological flows with strongly variable transport properties. *Phys. Earth Planet. Inter.* 140, 293–318. doi: 10.1016/j.pepi.2003.09.006

Glazner, A. F., Bartley, J. M., Coleman, D. S., Gray, W., and Taylor, R. Z. (2004). Are plutons assembled over millions of years by amalgamation from small magma chambers? *GSA Today* 14, 4–11. doi: 10.1130/1052-5173(2004)014<0004:APAOMO>2.0.CO;2

Gorbatov, A., Domiguez, J., Suarez, G., Kostoglodov, V., and Gordeev, E. (1999). Tomographic imaging of the P-wave velocity structure beneath the Kamchatka peninsula. *J. Geophys. Res.* 137, 269–279. doi: 10.1046/j.1365-246X.1999.00801.x

Gorbatov, A., Fukao, Y., Widiyantoro, S., and Gordeev, E. (2001). Seismic evidence for a mantle plume oceanward of the Kamchatka-Aleutian trench junction. *Geophys. J. Int.* 146, 282–288. doi: 10.1046/j.0956-540x.2001.01439.x

Grocke, S. B., de Silva, S. L., R., and Iriarte, J. M., Cottrell, L.E. (2017). Catastrophic Caldera-Forming (CCF) monotonous silicic magma reservoirs: geochemical and petrological constraints on heterogeneity, magma dynamics, and eruption dynamics of the 3·49 Ma Tara Supereruption, Guacha II Caldera, SW Bolivia. *J. Petrol.* 58, 227–260. doi: 10.1093/petrology/egx012

Gualda, G. A. R., Ghiorso, M. S., Lemons, R. V., and Carley, T. L. (2012). Rhyolite-MELTS: a modified calibration of MELTS optimized for silica-rich, fluid-bearing magmatic systems. *J. Petrol.* 53, 875–890. doi: 10.1093/petrology/egr080

Halliday, A. N., Davidson, J. P., Hildreth, W., and Holden, P. (1991). Modelling the petrogenesis of high Rb/Sr silicic magmas. *Chem. Geol.* 92, 107–114. doi: 10.1016/0009-2541(91)90051-R

Hawkesworth, C. J., Koloskov, A., Maury, R. C., and Bellon, H. (1997). Trace element and Sr-Nd-Pb isotopic constraints on a three-component model of Kamchatka Arc petrogenesis. *Geochim. Cosmochim. Acta* 61. 577–600. doi: 10.1016/S0016-7037(96)00349-3

Hildreth, W., and Moorbath, S. (1988). Crustal contributions to arc magmatism in the Andes of Central Chile. *Contribut. Mineral. Petrol.* 98, 455–489. doi: 10.1007/BF00372365

Hourigan, J. K., Brandon, M. T., Soloviev, A. V., Kirmasov, A. B., Garver, J. I., Stevenson, J., et al. (2009). Eocene arc-continent collision and crustal consolidation in Kamchatka, Russian Far East. *Am. J. Sci.* 309, 333–396. doi: 10.2475/05.2009.01

Huber, C., Bachmann, O., and Dufek, J. (2011). Thermo-mechanical reactivation of locked crystal mushes: melting-induced internal fracturing and assimilation processes in magmas. *Earth Planet. Sci. Lett.* 304, 443–454. doi: 10.1016/j.epsl.2011.02.022

Hudak, M. R., and Bindeman, I. N. (2008). Conditions of pinnacle formation and glass hydration in cooling ignimbrite sheets from H and O isotope systematics at Crater Lake and the Valley of Ten Thousand Smokes. *Earth Planet. Sci. Lett.* 500, 56–66. doi: 10.1016/j.epsl.2018.07.032

Hughes, G. R., and Mahood, G. A. (2008). Tectonic controls on the nature of large silicic calderas in volcanic arcs. *Geology* 36, 627–630. doi: 10.1130/G24796A.1

Ito, K., and Kennedy, G. C. (1971). An experimental study of the basalt-garnet granulite-eclogite transition. *Struct. Phys. Properties Earth's Crust* 14, 303–314.

Jicha, B. R., and Jagoutz, O. (2015). Magma production rates for intraoceanic arcs. *Elements Vol.* 11, 105–112. doi: 10.2113/gselements.11.2.105

Jicha, B. R., Singer, B. S., and Sobol, P. (2016). Re-evaluation of the ages of $^{40}Ar/^{39}Ar$ sanidine standards and supereruptions in the western U.S. using a Noblesse multi-collector mass spectrometer. *Chem. Geol.* 431, 54–66. doi: 10.1016/j.chemgeo.2016.03.024

Karakas, O., Degruyter, W., Bachmann, O., and Dufek, J. (2017). Lifetime and size of shallow magma bodies controlled by crustal-scale magmatism. *Nat. Geosci.* 10:446. doi: 10.1038/ngeo2959

Kimura, J.-I., Nagahashi, Y., Satoguchi, Y., and Chang, Q. (2015). Origins of felsic magmas in Japanese subduction zone: Geochemical characterizations of tephra from caldera-forming eruptions <5 Ma: origin of caldera eruptions in Japan. *Geochem. Geophys. Geosyst.* 16, 2147–2174. doi: 10.1002/2015GC005854

Kimura, J.-I., and Stern, R. J. (2008). "Neogene volcanism of the Japan island arc: the K-h relationship revisited," in eds J. E. Spencer and S. R. Titley *Ores and Orogenesis: Circum-Pacific Tectonics, Geologic Evolution, and Ore Deposits* (Tucson, AZ: Arizona Geological Society Digest), 187–202.

Konstantinovskaia, E. A. (2001). Geodynamics of an Early Eocene arc-continent collision reconstructed from the Kamchatka Orogenic Belt, NE Russia. *Tectonophysics* 325, 87–105. doi: 10.1016/S0040-1951(00)00132-3

Kraevoi, Y., Okhapkin, V. G., and Serezhnikov, A.I. (1976). Results from Hydrogeological and Geothermal Studies in the Bol'she- Bannaya and Karymchina Hydrothermal Systems, Gidrotermal'nye sistemy i termal'nye polya Kamchatki (Hydrothermal Systems and Thermal Fields of Kamchatka), Vladivostok: Far Eastern Scientfic Center, *USSR Academy of Sciences Proceedings*, 179–211.

Kuiper, K. F., Deino, A., Hilgen, F. J., Krijgsman, W., Renne P. R., and Wijbrans, J. R. (2008). Synchronizing rock clocks of Earth history. *Science* 320, 500–504. doi: 10.1126/science.1154339

Lander, A. V., and Shapiro, M. N. (2007). The Origin of the modern Kamchatka zone. Volcanism and Subduction: the Kamchatka Region. *Geophys. Monogr. Ser.* 172, 57–64. doi: 10.1029/172GM05

Lee, C. T. A., Cheng, X., and Horodyskyj, U. (2006). The development and refinement of continental arcs by primary basaltic magmatism, garnet pyroxenite accumulation, basaltic recharge and delamination: insights from the Sierra Nevada, California. *Contrib. Mineral. Petrol.* 151, 222–242. doi: 10.1007/s00410-005-0056-1

Leonov, V. L., and Rogozin, A. N. (2007). Karymshina, a giant supervolcano Caldera in Kamchatka: boundaries, structure, volume of pyroclastics. *Volcanol. Seismol.* 1, 296–309. doi: 10.1134/S0742046307050028

Lipman, P. W. (2007). Incremental assembly and prolonged consolidation of Cordilleran magma chambers. *Geosphere* 3, 42–70. doi: 10.1130/GES00061.1

Lipman, P. W., O. A., Bogatikov, A. A., Tsvetkov, Gazis, C., Gurbanov, A. G., Hon, K., et al. (1993). 2.8-Ma ash-flow caldera at Chegem River in the northern Caucasus Mountains (Russia), contemporaneous granites, and associated ore deposits. *J. Volcanol. Geotherm. Res.* 57, 85–124. doi: 10.1016/0377-0273(93)90033-N

Loewen, M., and Bindeman, I. N. (2016). Oxygen isotope thermometry reveals high magmatic temperatures and petrogenetic differences between hot-dry Yellowstone/ Snake River Plain and Icelandic rhyolites compared to cold-wet systems. *Am. Mineral.* 101, 1222–1227. doi: 10.2138/am-2016-5591

Loewen, M. W., and Kent, A. J. (2012). Sources of elemental fractionation and uncertainty during the analysis of semi-volatile metals in silicate glasses using LA-ICP-MS. *J. Anal. At. Spectrom.* 27, 1502–1508. doi: 10.1039/c2ja30075c

Miller, C. F., McDowell, S. M., and Mapes, R. W. (2003). Hot and cold granites? Implications of zircon saturation temperatures and preservation of inheritance. *Geology* 31, 529–532. doi: 10.1130/0091-7613(2003)031<0529:HACGIO>2.0.CO;2

Min, K., Mundil, R., Renne, P. R., and Ludwig, K. R. (2000). A test for systematic errors in 40Ar/39Ar geochronology through comparison with U/Pb analysis of a 1.1-Ga rhyolite. *Geochim. Cosmochim. Acta* 64, 73–98. doi: 10.1016/S0016-7037(99)00204-5

Nizkous, I., Kissling, E., Sanina, I., Gontovaya, L., and Levina, V. (2007). Correlation of kamchatka lithosphere velocity anomalies with subduction processes. volcanism and subduction: the Kamchatka region. *Geophys. Monogr. Am. Geophys. Union* 172, 97–106. doi: 10.1029/172GM09

Ponomareva, V., Bubenshchikova, N., Portnyagin, M., Zelenin, E., Derkachev, A., Gorbarenko, S., et al. (2018). Large-magnitude Pauzhetka caldera-forming eruption in Kamchatka: astrochronologic age, composition and tephra dispersal. *J. Volcanol. Geotherm. Res.* 336, 1–12. doi: 10.1016/j.jvolgeores.2018.10.006

Ponomareva, V., Melekestsev, I., Braitseva, O., Churikova, T., Pevzner, M., and Sulerzhitsky, L. (2007). Late pleistocene-holocene volcanism on the kamchatka peninsula, northwest pacific region. volcanism and subduction: the Kamchatka Region. *Geophys. Monogr. Am. Geophys. Union* 172, 165–198. doi: 10.1029/172GM15

Portnyagin, M., Hoernle, K., Plechov, P., Mironov, N., and Khubunaya, S. (2007). Constraints on mantle melting and composition and nature of slab components in volcanic arcs from volatiles (H2O, S, Cl, F) and trace elements in melt inclusions from the Kamchatka Arc. *Earth Planet. Sci. Lett.* 255, 53–69. doi: 10.1016/j.epsl.2006.12.005

Prueher, L. M., and Rea, D. K. (2001). Tephrochronology of the Kamchatka±Kurile and Aleutian arcs: evidence for volcanic episodicity. *J. Volcanol. Geotherm. Res.* 106, 67–84. doi: 10.1016/S0377-0273(00)00266-3

Qi, H., Coplen, T. B., Gehre, M., Vennemann, T. W., Brandt, W. A., Geilmann, H., et al. (2017). New biotite and muscovite isotopic reference materials, USGS57 and USGS58, for d2H measurements-a replacement for NBS 30. *Chem. Geol.* 657:89–99. doi: 10.1016/j.chemgeo.2017.07.027

Rapp, R. P., and Watson, E. B. (1995). Dehydration melting of metabasalt at 8-32 kbar: implications for continental growth and crust-mantle recycling. *J. Petrol.* 36, 891–931. doi: 10.1093/petrology/36.4.891

Rogozin, A., Leonov, L., and Sobolevskaya, O. (2015). "Bol'she-bannaya hydrothermal system: new thermometric survey data and the position of the system relative to Karymshina Caldera (South Kamchatka),"in *Proceedings World Geothermal Congress* 2015 Melbourne, Australia, 1–7.

Rudnick, R. L., and Gao, S. (2003). "Composition of the continental crust," in *The Crust. Treatise on Geochemistry,* ed R. L. Rudnick (Oxford: Elsevier-Pergamon), 1–64.

Schmidt, M. (1992). Amphibole composition in tonalite as a function of pressure: an experimental calibration of the Al-in-hornblende barometer. *Contrib. Mineral. Petrol.* 110, 304–310. doi: 10.1007/BF00310745

Scholl, D. (2007). Viewing the tectonic evolution of the kamchatka-aleutian (KAT) connection with an alaska crustal extrusion perspective. volcanism and subduction: the kamchatka region. *Geophys. Monogr. Am. Geophys. Union* 172, 3–35. doi: 10.1029/172GM03

Seligman, A., Bindeman, I. N., Jicha, B., Ellis, B., Leonov, V. L., and Ponomareva, V. V. (2014). Recognizing subtle evidence for silicic magma derivation from petrochemically-similar arc crust: isotopic and chemical evidence for the bimodal volcanic series of Gorely Volcanic Center, Kamchatka. *Russia J. Petrol.* 55, 1561–1594. doi: 10.1093/petrology/egu034

Seligman, A. N., Bindeman, I. N., Van Eaton, A., and Hoblitt, R. (2018). Isotopic insights into the degassing and secondary hydration of volcanic glass from the 1980 eruptions of Mount St. *Helens. Bull. Volcanol.* 80:4. doi: 10.1007/s00445-018-1212-6

Sheimovich, V. S., and Golovin, D. J. (2003). Age of silicic volcanic rocks in the Bolshoy Banny springs. *Volcanol. Seismol.* 1, 21–25

Sheimovich, V. S., and Khatskin, S. V. (1996). Rhyodacitic magmatic formation of southeastern Kamchatka. *Volcanol. Seismol.* 5, 99–105.

Sheimovich, V. S., and Patoka, M. G. (1989). *Geologicheskoe Stroenie Zon Aktivnogo Kainozoiskogo Vulkanizma (The Geological Structure of Zones of Active Cenozoic Volcanism)*. Moscow: Nedra publisher.

Shipley, N. K. (2011). *Isotopic and Petrologic Investigation and Model of Genesis of Large-Volume High-Silica Rhyolites in Arc Environments: Karymshina Caldera, Kamchatka, Russia*. MS Thesis University of Oregon, 76p. Available online at: http://hdl.handle.net/1794/12187

Simakin, A. G., and Bindeman, I. N. (2012). Remelting in caldera and rift environments and the genesis of hot, "recycled" rhyolites. *Earth Planet Sci. Lett.* 337–338, 224–235. doi: 10.1016/j.epsl.2012.04.011

Simon, A., Yogodzinski, G. M., Robertson, K., Smith, E., Selyangin, O., Kiryukhin, A., et al. (2014). Evolution and genesis of volcanic rocks from Mutnovsky Volcano, Kamchatka. *J. Volcanol. Geotherm. Res.* 286, 116–137. doi: 10.1016/j.jvolgeores.2014.09.003

Taran, Y. A., Pokrovsky, B. G., and Volynets, O. N. (1997). Hydrogen isotopes in hornblendes and biotites from Quaternary volcanic rocks of the Kamchatka-Kurile arc. *Geochem. J.* 31, 203–221. doi: 10.2343/geochemj.31.203

Tatsumi, Y. (2005). The subduction factory: how it operates in the evolving earth. *GSA Today* 15:7. doi: 10.1130/1052-5173(2005)015[4:TSFHIO]2.0.CO;2

Taylor, H. P. Jr. (1986). "Igneous rocks:II. Isotopic case studies of circumpacific magmatism," in *Stable Isotopes in High Temperature Geological Processes*, Vol. 16, eds J. W. Valley, H. P. Taylor Jr, and J. R. O'Neil (Washington, DC: Mineralogical Society of America; American Geophysical Union), 273–316.

Taylor, S. R., and McLennan, S. M. (1995). The geochemical evolution of the continental crust. *Rev. Geophys.* 33, 241–265. doi: 10.1029/95RG 00262

Tuttle, O. F., and Bowen, N. L. (1958). *Origin of Granite in the Light of Experimental Studies in the System.* Memoir: Geological Society of America, 74

Vinogradov, V. I. (1995). Isotopic evidence of the conversion of oceanic crust to continental crust in the continent-ocean transition zone of Kamchatka. *Geochem. Int.* 32, 70–109.

Vinogradov, V. I., Buyakaite, M. I., Goroshenko, G. L., Lukanin, A. O., and Pokrovsky, B. G. (1991). Isotope and geochronological features of deeply metamor- phosed rocks of Ganal Massif in Kamchatka. *Trans. Russ. Acad. Sci. Earth Sci. Sect.* 318:929–936.

Vinogradov, V. I., V. S., and Grigoriev, and, B. G., Pokrovsky (1986). "Isotopic composition of the oxygen and strontium in the rocks of the Kurile-Kamchatka island arc-key for some genetic constructions(in Russian)," in *Evolution of the System Crust-Mantle*, ed Y. A. Shukolyukov (Moscow: Nauka, Acad.Sci.USSR), 78–102.

Vogel, T., Patino, L. C., Eaton, J. K., Valley, J. W., Rose, W. I., Alvarado, G. E., et al. (2006). Origin of silicic magmas along the Central American volcanic front:

genetic relationship to mafic melts. *J. Volcanol. Geotherm. Res*. 156, 217–228. doi: 10.1016/j.jvolgeores.2006.03.002

Vogt, K., Gerya, T. V., and Castro, A. (2012). Crustal growth at active continental margins: numerical modeling. *Phys. Earth Planet. Interiors* 192–193, 1–20. doi: 10.1016/j.pepi.2011.12.003

Volynets, O. (1994). Geochemical types, petrology, and genesis of Late Cenozoic volcanic rocks from the Kurile-Kamchatka island-arc system. *Int. Geol. Rev*. 36, 373–405. doi: 10.1080/00206819409465467

Waters, L. E., and Lange, R. A. (2017). Why aplites freeze and rhyolites erupt: controls on the accumulation and eruption of high-SiO2 (eutectic) melts. *Geology* 45, 1019–1022. doi: 10.1130/G39373.1

Watson, E. B., and Harrison, T. M. (1983). Zircon saturation revisited: temperature and compositional effects in a variety of crustal magma types. *Earth Planet. Sci. Lett.* 64, 295–304. doi: 10.1016/0012-821X(83)90211-X

Watts, K. E., Bindeman, I. N., and Schmitt, A. K. (2011). Large-volume rhyolite genesis in caldera complexes of the Snake River Plain: Insights from the Kilgore Tuff of the Heise Volcanic Field, Idaho, with comparison to Yellowstone and Bruneau-Jarbidge Rhyolites. *J. Petrol.* 52, 857–890. doi: 10.1093/petrology/egr005

Watts, K. E., John, D. A., Colgan, J. P., Henry, C. D., Bindeman, I. N., and Schmitt, A. K. (2016). Probing the volcanic–plutonic connection and the genesis of crystal-rich rhyolite in a deeply dissected supervolcano in the nevada great basin: source of the late eocene caetano tuff. *J Petrol.* 57, 1599–1644. doi: 10.1093/petrology/egw051

Winter, J. D. (2010). *Principles of Igneous and Metamorphic Petrology 2nd Edn*. London: Pearson Publisher, 720.

Wyllie, P. J. (1984). Constraints imposed by experimental petrology on possible and impossible magma sources and products. *Philos. Trans. R. Soc. Lond. A* 310, 439–456. doi: 10.1098/rsta.1984.0003

Conflict of Interest Statement: The authors declare that the research was conducted in the absence of any commercial or financial relationships that could be construed as a potential conflict of interest.